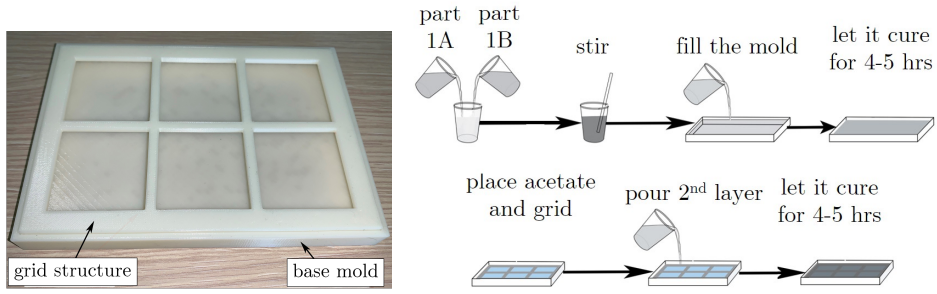

(a) (b)

Figure 6.2: (a) 3D printed mold and grid structure for building the SoftPad, (b) a scheme of the complete process flow to develop a SoftPad.

with reduced distances. Also the total number of modules depends on the objects, which should not cover the entire SoftPad. In this work, we selected size and number of modules as the best compromise for the objects in the experimental set. The device that we built was meant to be a prototype to validate the effectiveness of the devised grasping strategy and thus was specifically suitable for the set of objects that we chose and exploited in Section 6.3.

For developing the SoftPad, we followed similar guidelines as those described in [144]. The process started by designing a mold consisting of a base and a grid both realized in ABS material, as shown in Fig. 6.2a. The material used for the SoftPad was the EcoFlex silicone (Smooth-On Inc., USA) with shore hardness of 00-30[1]. The Ecoflex silicone is a platinum-catalyzed silicone and is versatile and easy to use. It comes with two parts defined as A and B. The optimal mixing ratio to achieve a smooth and well cured elastomer is $A/B = 1$.

The molding process is shown in Fig. 6.2b. The first layer, that serves as a base for the SoftPad, was cast with silicone as per the predefined height. Once the filling was completed, the elastomer was left to cure for 4-5 hours. After the fully cured silicone structure was achieved, the subsequent step was to divide the structure into a number of small squares (which serve as soft modules) by using the grid part. To define a pneumatic channel in each square, a 45×45 mm piece of acetate was placed on top of the first layer. The purpose of acetate was to allow the silicone elastomer to flow around it without adhering, establishing an inner channel. Lastly, the second layer of silicone was cast on

[1] https://www.smooth-on.com/tb/files/ECOFLEX_SERIES_TB.pdf

top of the acetate and the mold was filled as per the required height, which was 1.5 mm in our preliminary prototype. Again, the second layer had to cure for 4-5 hours. To avoid bubble formation, the two parts had to be mixed and stirred very thoroughly for at least 3 minutes, and the curing phase had to occur in a heating chamber.

A height difference between the base and the upper layer of the SoftPad enables the modules to be very soft on the top and considerably rigid on the other side, hence, minimizing the downward inflation. In our prototype, to further reduce downward inflation and enable a smooth upward inflation, a sheet of neoprene was embedded inside the base layer.

High strength silicone tubes SPX-60 FB Versilon (Saint-Gobain Performance Plastics, FR) were placed in each module by inserting them through a small hole made with pointed end tweezers at the level of the acetate. Liquid silicone was put around the circumference of the tubes to avoid air leaks. The tubing was connected to the Pneumaticbox, that was used to control the inflation and deflation of the modules. The Pneumaticbox is a control system developed to enable fast and real-time control of pneumatic systems. It can provide up to eight independently controlled channels, each equipped with two discrete valves for inflation and deflation, and a differential pressure sensor for reading the channel air pressure. A separate pressure sensor was used to read the supply pressure which was shared by all the channels. All pressure sensors and valves were connected to a BeagleBone®Black (BeagleBoard.org, USA) embedded computer, which is the main processing unit for the Pneumaticbox.

6.1.2 FEM simulation

To analyze the main structural properties of the SoftPad, a Finite Element Method (FEM) simulation has been set up using Comsol Multiphysics® (Comsol Inc., USA) software. For the sake of clarity, only one pneumatic module was considered. We acknowledge that the uncertainties in the manufacturing process could lead to some variations among different modules (slightly different thickness, dimensions, material heterogeneity, etc.). However, the differences that we observed in the modules realized for our tests were not significant with respect to the level of precision and sensitivity required by the system.

The geometrical model of the SoftPad consists of a mesh with 5106 thethraedral elements. A surface pressure loading p is applied to the lower surface of the pneumatic module, to simulate the inflating pressure, while its external boundaries are blocked with a fixed constraint. We assumed an hyperelastic material, nearly incompressible with quadratic volumetric strain energy [145].

Since data available in the literature about mechanical properties of the selected mate-

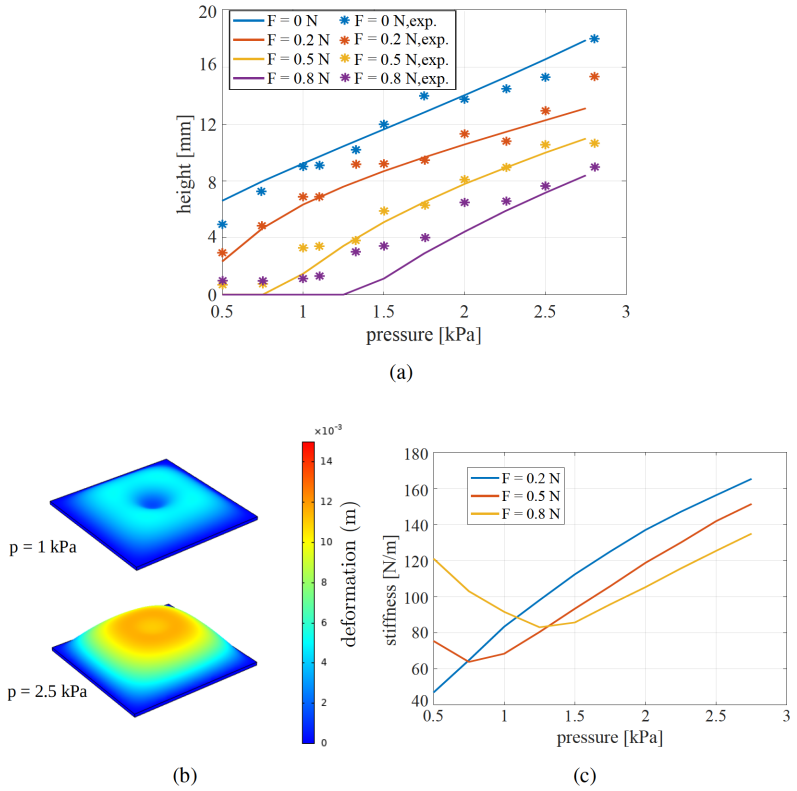

Figure 6.3: FEM model of the SoftPad. (a) Height of a module as a function of the inflating pressure, comparison between simulation results (continuous curves) and experimental measurements obtained using a load cell (coloured dots). Each colour identifies a different force applied to the module. (b) Deformation (in m) of the module for two different inflating pressures (1 kPa, 2.5 kPa), and an external load $F = 0.5$ N applied in the center. (c) Equivalent mean stiffness of a module as a function of inflating pressure: simulation results for different external forces.

rial vary in a wide range and the manufacturing process may be affected by uncertainties, a first set of simulations was realized to identify material properties (Young's modulus, Shear Modulus, Poisson's ratio, bulk modulus, and mass density). In such simulations, we analyzed the relationship between the inflating pressure and the soft module deformation and compared it with values measured on a real module. Material parameters were selected in order to minimize the difference between experimental values and numerical simulation. In these simulations, a constant pressure value varying from 0.5 to 2.8 kPa

was applied and the overall displacement in the center of the pneumatic module was evaluated. Pressure values varying in the same range were applied to the real SoftPad and the corresponding physical deformation was measured. The indicated minimum and maximum pressure values were chosen by observing the SoftPad behavior, as explained in Section 6.3. Results are shown in Fig. 6.3a. In the same figure, also simulated and experimental results obtained by applying an external force in the center of the module, with different force magnitude values, are reported. The used FEM model shows good capabilities of predicting the module deformations, except from when it undergoes large deformations due to high forces.

Other simulations were conducted to study how the sensitive area of a module changes with respect to the inflating pressure. The sensitive area of a module can be obtained by considering its inflatable area and the height to which it is inflated. In our case, it approximately corresponds to the surface of a spherical cap with a square basis having side l proportional to the inflating pressure. For the analyzed configuration, l varies from ≈ 20 mm for low pressures (0.5 kPa) to ≈ 45 mm for higher pressures (2.8 kPa). Fig. 6.3b shows the module deformation (in m) obtained for two different inflating pressures (p =1 and p =2.5 kPa) when simulating the application of an external normal force $F = 0.5$ N in a central circular area with radius $r = 5$ mm. Note that the deformation around the borders is limited.

A third set of simulations was carried out to estimate the mean equivalent stiffness in the vertical direction of each pneumatic module. To this aim, a vertical force was applied on a circular area with a radius $r = 1$ cm in the center of the module, with an equivalent resulting magnitude $F = \{0.2, 0.5, 0.8\}$ N. We measured the corresponding deformation of the module for different inflating pressure values and compared the displacement in the vertical direction of the module center, h_{load}, with the value obtained without external forces, h_{free}. We therefore evaluated the equivalent stiffness as $k = F/(h_{free} - h_{load})$. Obtained results are reported in Fig. 6.3c. When the pressure value is sufficiently high or the applied force is sufficiently low, increasing the inflating pressure p we observe, as expected, an increase in the equivalent stiffness k. In this cases, a decrease in the equivalent stiffness as the applied force magnitude increases can be furthermore observed. Instead, for high forces applied to modules at low pressure values, the overall module deformation caused by the force application is such that the upper silicone layer contacts the lower one and the corresponding stiffness is therefore higher. This effect is visible when forces $F = 0.5$ N and $F = 0.8$ N are applied.

From the sensing point of view, varying the inflating pressure allows to change measurement range and sensitivity of the device. For higher inflating pressures, for example, modules are less sensitive to external deformations, because they are stiffer,

and the same mass would generate a smaller deformation in the inflated module, thus, lighter objects might not be detected. However, the more a module is inflated the larger is the full scale of detectable weights. For higher inflating pressures, modules can resist higher forces and thus detect heavy objects without collapsing (see the simulation results in Fig. 6.3a: for high force magnitudes and low pressure values, the upper layer falls on the lower layer and its height drops to zero). Similarly, a thicker upper layer corresponds to a less sensitive module and a higher full scale.

We can express the sensitivity of our device as the minimum mass that can be detected over a module. This depends on the sensitivity of the pressure sensors, but also on the thickness of the modules upper layer and on the inflating pressure. In the prototype here described, for example, with an inflating pressure of 1.1 kPa, which is the pressure value used during the experimental evaluation, the minimum detectable mass experimentally found is around 6 g. The corresponding generated deformation is not perceivable by eyes.

6.2 Grasping with the SoftPad

This section describes a grasping strategy that allows a rigid gripper to perform top-grasps of objects placed over the SoftPad. Pressure readings coming from the SoftPad are used *i*) in the grasp planning phase to estimate the pose and the center of mass of the object to be grasped, and *ii*) during grasp execution to detect the contact between the robotic gripper and the SoftPad. In both phases, the algorithm is based on the evaluation of the pressure increments ΔP_i in each module i.

6.2.1 Grasp planning

When an object is placed on the SoftPad, we assume that the modules that are in contact with the object are those in which an increment of pressure with respect to the initial inflating value higher than a certain threshold t_o is detected. Note that, when a variation of pressure occurs in a module, it is not possible to estimate the exact location of the object over the module itself from the sole pressure measurement. In fact, the object could be covering the whole module surface or a smaller portion of it: since the only information we rely on is given by pressure measurements, we cannot distinguish these two cases. Thus, the modules size should be chosen on the basis of the size of the objects that have to be grasped in a certain application. If the objects are too small and cover just one module, most of the benefits of using the SoftPad would be lost.

The outcomes of the grasp planning phase are the center and direction of grasp for a rigid parallel-jaw gripper. To compute them, first all the modules are inflated to the same

pressure, and then the center of mass of the object is computed.

6.2.1.1 Initial inflating procedure

Before starting to use the SoftPad, it should be inflated to a desired initial pressure. To guarantee the proper functioning of the algorithm and the repeatability of the experiments, it is important that each module is inflated at the same initial inner pressure. This ensures that the heights of the six modules are the same, and thus the object is not tilted when placed on the SoftPad. Moreover, since the algorithm is based on the evaluation of the variations of pressure with respect to the inflating value, these variations would be more complex to compare if computed starting from quite different inflating values. For these reasons, if before the placement of the object the pressure in one or more modules differs from the selected initial pressure of a value greater than a certain tolerance t_{adj}, an automatic procedure will inflate/deflate the corresponding module(s) accordingly. The tolerance t_{adj} should be chosen as a compromise between accuracy and length of the adjustment phase.

After the adjustment procedure is finished, the current pressure of each module is measured and saved as a reference value. Then, an object can be placed over the SoftPad and its center of mass can be evaluated starting from the new pressure readings, as explained in the following.

6.2.1.2 Estimation of center of mass

We consider the object as a discrete system composed of as many masses as the number of modules in contact with the object, each of them placed in the center of the corresponding module (see Fig. 6.4a). The center of mass of the object is estimated by computing a weighted average of the variations of pressure ΔP_i, $i = 1, \ldots, N$, where N is the number of modules in contact with the object. The resulting point is called *Pressure-based center of mass*, or *PCOM*, and is computed as:

$$x_{PCOM} = \frac{\sum_{k=1}^{N}(\Delta P_i x_i)}{\sum_{k=1}^{N} \Delta P_i}, \; y_{PCOM} = \frac{\sum_{k=1}^{N}(\Delta P_i y_i)}{\sum_{k=1}^{N} \Delta P_i}. \tag{6.1}$$

Considering the reference frame shown in Fig. 6.4a, x and y range in a discrete set of values: $x_i = \{0.5, 1.5, 2.5\}$ and $y_i = \{0.5, 1.5\}$. Note that, from these assumptions, the two objects in Fig. 6.4b have the same *PCOM*, even if they have different shapes. In Fig. 6.4b-(3), module 1 is only partially covered by the object and this information is taken into account thanks to the fact that most of the pressure variation is sensed in module 4 (Fig. 6.4b-(1)), as the object is shifted towards it. In Fig. 6.4b-(4), the object is

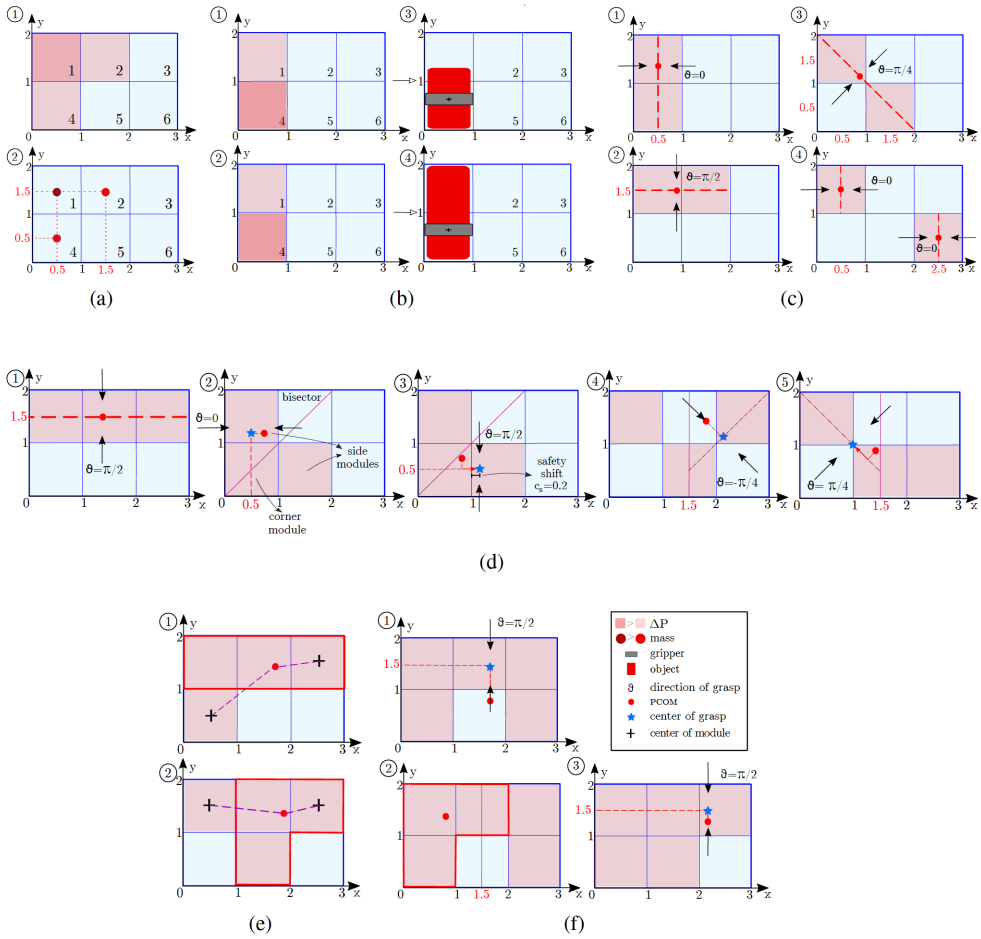

Figure 6.4: Illustration of the working principles of the SoftPad based grasp planning strategy, from simpler to more complex cases. Note that while in (a) and (b) different shades of pink are used to denote different ΔP to let the user familiarize with the $PCOM$ computation, this detail is omitted in other figures for the sake of clarity.

equally placed over the two modules, but has a mass distribution that generates a higher pressure variation in module 4 (Fig. 6.4b-(2)).

6.2.1.3 Computation of center and direction of grasp

To identify the grasp, two parameters are required: a point on the object over which the gripper's center should be aligned (*center of grasp* or COG) and an angle θ identifying the orientation of the gripper (*direction of grasp*). Angle θ ranges from $-\pi/4$ to $\pi/2$, considering that it is equal to 0 when the direction of grasp is parallel to the x-axis of the SoftPad.

As a first step, the planner counts the number N of modules touched by the object. If the N modules are not adjacent (not even in diagonal), the algorithm assumes that there are at least two objects on the SoftPad, since bridge-shaped objects are not taken into account. In this case, the algorithm treats them separately, to grasp them in sequence.

Depending on the value of N, COG and θ are evaluated with different procedures. The SoftPad that we designed has six modules, this is why in the following we describe six different cases, depending on the number of modules touched by the object. However, the described computations can easily be extended to more modules, as more complex cases can be treated, with some adjustments, as simpler cases.

• ***N* = 1.** The COG corresponds to the center of the module, e.g., (0.5, 1.5) for module 1. The direction of the grasp can be chosen by default, e.g., $\theta = 0$. Note that the 1-module object is a limit case of our algorithm, because, as we wrote at the beginning of this section, we cannot retrieve information about its shape.

• ***N* = 2.** The algorithm detects if the object is horizontal, vertical, or diagonal. As shown in Fig. 6.4c, the COG corresponds to the $PCOM$ computed from Eq. (6.1), which is always on the major axis of the object (i.e., the axis linking the centers of the two modules, depicted as a dashed red line). The direction of the grasp is perpendicular to the major axis. For example, if the object is vertical, $\theta = 0$ and the $PCOM$ has the same x of the center of the two modules, while the y depends on the weight distribution of the object.

• ***N* = 3.** As shown in Fig. 6.4d-(1), if the object is horizontal, the COG corresponds to the *PCOM* and the direction of the grasp is vertical ($\theta = \pi/2$).

If the three modules are in a "corner-shaped" configuration as in Figs. 6.4d-(2)..(5), the COG may not coincide with the $PCOM$. Since we are considering a discrete system of masses, when they are not aligned, the $PCOM$ can also fall outside of the involved modules. The COG, instead, has to be on the axis of one module belonging to the object to allow the gripper to grasp the object.

Considering Figs. 6.4d-(2)(3), let us call *corner module* the one in the middle, *side modules* the other two, and *bisector* the line starting from the outer corner of the corner module and dividing the object in two equal parts. Since the exact shape around the corner is not known, it is safer to grasp along one of the two side modules rather than

on the corner module. If the $PCOM$ is in one of the side modules, it is projected on the axis of the side module itself (Fig. 6.4d-(2)). If the $PCOM$ falls on the corner module, as in Fig. 6.4d-(3), the position of the ***COG*** is obtained by projecting the $PCOM$ on the closest axis of the corner module itself and then shifting it towards the nearest side module. A safety margin c_s is thus added either to the x (Fig. 6.4d-(3)) or to the y of the $PCOM$. This *safety shift* allows the gripper to move from a potentially unsafe position (i.e., the corner of the object). In our experiments we used $c_s = 0.2$. The direction of the grasp is the direction of the projection on the axis.

A similar reasoning applies for cases like those shown in Figs. 6.4d-(4)(5), where it is difficult to do assumptions on the object shape along the diagonal parts. In these cases the bisector is considered vertical and the direction of the grasp can be either $\theta = \pi/2$ or $\theta = \pm\pi/4$, depending on the direction of projection of the $PCOM$. In these configurations, the $PCOM$ can also fall outside of the object, as in Fig. 6.4d-(4). In this case, it is projected on the axis of the nearest module (evaluated with respect to the bisector). When the projection of the $PCOM$ falls on the axis of the corner module, as in Fig. 6.4d-(5), it is preferable to move the COG to the nearest corner of the side module. In general, when dealing with corner-shaped objects, the use of shifts like the ones shown in Figs. 6.4d-(3)(5) allows us to ensure a safer grasp moving the gripper away from a potentially critical position.

To summarize, as for the 2-modules object case, in which the direction of the grasp is perpendicular to its major axis, when the number of modules increases we applied the same reasoning, considering as "major axis" the one passing through the center of grasp (COG). Indeed, we consider as direction of the grasp the direction of the projection of $PCOM$, as detailed in Fig. 6.4.

• ***N* = 4.** A limit case is the object occupying a square of 2×2 modules. This case, similarly to the 1-module case, is treated choosing the direction of the grasp by default, while the COG is the center of the square. In all other cases, to simplify the algorithm and make it as scalable as possible, we do not consider one of the modules at the extremities and treat the object as it is 3-modules. The module which is not taken into account is the one whose center is the farthest from the $PCOM$ (see Fig. 6.4e), i.e., the one which affects less the $PCOM$ position. In this way, central modules (2 and 5 in Fig. 6.4a) are never removed and the original shape is changed only far from the COG, so that a safe grasp is always achieved. Taking Fig. 6.4e-(1) as example, after re-shaping the object as it is 3-modules object it appears as a rectangle. If the gripper tried to grasp it from module 1, it would hit the portion of object in module 4. However, since the removed module is always far from the $PCOM$ and thus from the COG, this will never happen.

• ***N* = 5.** The grasping strategy in this case depends on the position of the module

that is not touched by the object. When modules are in a horseshoe, if the $PCOM$ falls in the central modules 2 or 5 (as in Fig. 6.4f-(1)) the safest grasp is obtained projecting the $PCOM$ (thus placing the COG) to the axis of the central module that is covered by the object, because the weight of the object is well-balanced on the x-axis. If the $PCOM$ falls anywhere else, for the sake of simplicity and scalability all the cases can be reduced to a 3-modules object case. If $PCOM$ is on the left of the vertical bisector ($x_{PCOM} < 1.5$) modules 3 and 6 are removed (Fig. 6.4f-(2)), otherwise 1 and 4.

When modules occupy a 2×2 square plus a single module, if the $PCOM$ falls in the square, the direction of the grasp is vertical ($\theta = \pi/2$), $x_{COG} = x_{PCOM}$, and $y_{COG} = 1$. Otherwise, the COG is obtained by the projection of the $PCOM$ onto the axis of the single module (Fig. 6.4f-(3)).

• ***N* = 6.** The COG corresponds to the projection of the $PCOM$ on the major axis of the SoftPad, and the direction of the grasp is vertical ($\theta = \pi/2$).

In this work the number of modules is limited to 6, but the algorithm can be applied to SoftPads characterized by a higher number of modules. The complexity of the algorithm would increase with the number of modules, and thus appropriate arrangements are needed to face the scalability issue. For $N > 6$, the idea is always to evaluate only the area around the Pressure-based center of mass ($PCOM$), leading back the problem to simpler cases. As previously shown, when the number of involved modules increases, the algorithm can be simplified *i)* ignoring one or more modules (e.g., from $N = 4$ we obtain a $N = 3$ object), or *ii)* assuming that the object has an almost rectangular shape (e.g., from $N = 6$ to $N = 2$). For $N > 6$, the same reasoning can be applied. If the $PCOM$ of the object falls in a "square-shaped region", the algorithm will consider it as it was a big $N = 2$ rectangle. If the $PCOM$ of the object falls in a region with a more complex shape, the algorithm will ignore some modules as in case $N = 4$-L-shaped or $N = 5$-horseshoe. Fig. 6.5 summarizes the main steps of the grasp planning strategy.

The decision of increasing the number of modules of the SoftPad to obtain a higher spatial resolution depends on the desired level of accuracy and is required with objects with particularly complex shapes or when using very small grippers. According to the set of objects and the available gripper, the best solution is to find a compromise between resolution and simplicity of the device.

Note that the parameters (COG, c_s) computed as in this section are expressed in a reference frame where a unit corresponds to the side of a module (Fig. 6.4a). In this way, all computations can be generalized to SoftPads with modules of any size.

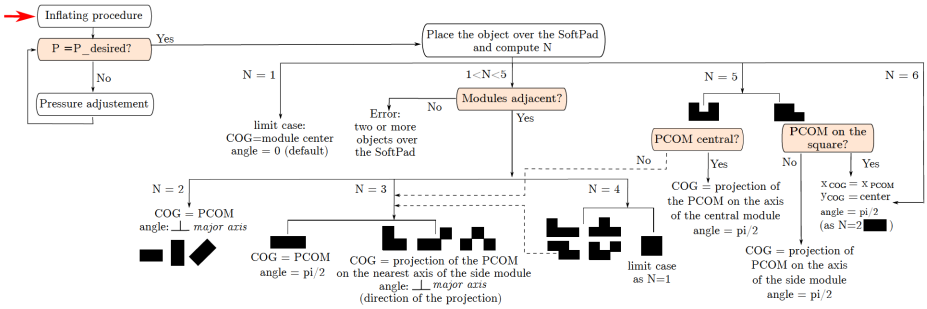

Figure 6.5: Diagram of the grasp planning algorithm that outputs center and direction of grasp. The red arrow shows the starting point. Pink squares represent if-statements. Dotted lines indicate that one case can be simplified and treated as if it involves a lower number of modules, by removing one or more of the side modules.

6.2.2 Grasp execution

After multiplying the components of the COG by the length of the module side, the obtained COG and θ are sent to a robot arm equipped with a rigid gripper, that moves toward the desired grasping pose over the object. Once it reaches the computed grasping pose, the gripper starts moving down towards the SoftPad. The advantage of having a soft surface underneath the objects is that we do not need to precisely control the vertical motion of the manipulator, since the fingers can safely touch the SoftPad and slide over it, after caging the object. As soon as the pressure in the SoftPad due to the contact with the gripper overcomes a threshold t_g, the arm is stopped and the gripper is closed to grasp the object.

The actual amount of sliding motion performed by the gripper fingers depends on object size and gripper opening. If, for example, the object to be grasped has a larger height than fingers' length, the gripper will start closing as soon as its center touches the object, as also in this case a variation of pressure is sensed by the SoftPad. If the object, instead, is not as tall as the fingers and does not cover the whole area of the module in the direction of grasp, as in Fig. 5.1c, there is free space between the object and the jaws. The gripper will thus cage the object and start closing after touching the SoftPad, performing a *surface-constrained grasp*, as it is called in the literature on environmental constraints exploitation [125].

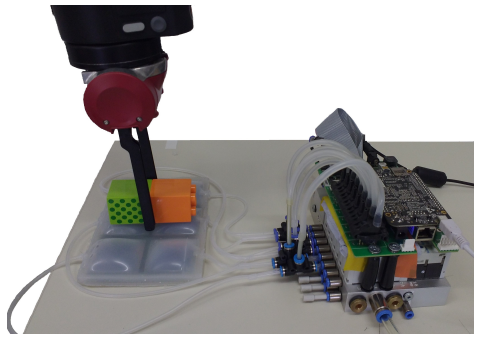

Figure 6.6: Experimental setup showing the Sawyer gripper grasping an object laying on the SoftPad.

6.3 Experiments

The grasp planning strategy described in Section 6.2 was tested for 14 different objects, covering most of the cases that the algorithm can account for. To perform the planned grasps, we used a Sawyer collaborative robot arm equipped with a parallel jaw gripper with 9.5 cm long fingers, as shown in Fig. 6.6. Depending on the object to be grasped, the gripper was mounted in three different ways, achieving a maximum width of $\{10, 6, 4\}$ cm respectively, and a corresponding minimum width of $\{4, 2, 0\}$ cm. During the experiments, the grasp execution was implemented as described in Section 6.2.2: the gripper was automatically positioned and oriented over the object according to the center and direction of grasp outputted by the grasp planner, then it went down towards the object and automatically closed as soon as the pressure threshold t_g was overcome, meaning that a contact between the gripper and the SoftPad was detected. The SoftPad inflation and reading, the robot controller, and the information exchange between the SoftPad and the robot were implemented within the ROS framework [146] and can be easily integrated within the main existing architectures.

At the beginning of each experimental session, the SoftPad was inflated to achieve a pressure of 1.1 kPa in each module, corresponding to a height of 9 mm. We observed that the range of possible inflating pressures goes from 0.5 to 2.8 kPa. For lower values, the SoftPad is almost deflated and the evaluation of the variation of pressure in each module is not feasible. For higher values, modules become too stiff and their shape is such that the object cannot be stably placed over them. For the initial pressure we chose an intermediate value in this range.

In the experiments, the threshold for the grasp planner was chosen so that it was

possible to detect one Lego Duplo piece (12.6 g, 42×31×31 mm) and it is $t_o = 0.05$ kPa. In general, this threshold should be selected based on the lightest item in the set of objects that need to be manipulated. The threshold for the initial phase of pressure adjustment was chosen as $t_{adj} = 0.03$ kPa, whereas the threshold for the detection of the contact between the gripper and the SoftPad was $t_g = 0.09$ kPa. Note that t_g must be chosen to accurately avoid any false positive due to oscillations of measurements, which during the contact detection would lead to close in advance the gripper. The value of t_g can be greater than t_o, because the impact of a rigid gripper moving towards the SoftPad is easier to detect, as it produces larger pressure variations. Raw pressure measurements from the Pneumaticbox were filtered using a running average filter of ten samples.

First, in a preliminary phase of the experimental evaluation all the possible combinations considered by the algorithm were tested simulating by software different pressure variations in the modules. Since the aim was only to verify the correctness of the algorithm, each trial ended after the computation of the grasp parameters, without then using the robot to grasp the objects.

In the following, two experiments are presented: one shows the detailed functioning of the grasp planning strategy and the working principles of the SoftPad, the other illustrates that the devised algorithm works for a variety of objects.

Experiment 1: Working principles of the grasping strategy

The functioning of the grasp planning strategy based on SoftPad readings is shown considering an object composed of three Lego Duplo pieces. Fig. 6.7a illustrates the planned grasp, whereas Fig. 6.8 reports pressure values for each module during the grasp execution phases: the initial adjustment of the internal pressure of the modules, the detection of the object, and the detection of the contact with the robot. As depicted in Fig. 6.4b, there are cases in which the planned grasp is similar for two different objects (cf. Section 6.2). Fig. 6.7b shows an example of this situation involving 2 adjacent modules. An object shifted towards module 1 and another object with the base centered between modules 1 and 2, but heavier in correspondence to module 1, are grasped similarly.

However, the SoftPad not only detects objects' features, but was primarily built for obtaining a safe gripper/environment interaction due to its intrinsic compliance. This aspect can also help to robustly grasp objects that cannot be picked up when laying on a rigid surface, as depicted in Fig. 6.9. This figure shows the outcome of an experimental trial demonstrating that having a soft surface under the objects to be grasped not only adds safety with respect to the robot/environment interaction, but also allows to perform

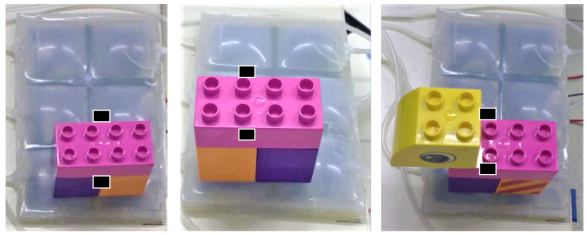

(a) (b)

Figure 6.7: (a) Simple object (weight = 38 g) laying on two adjacent modules: planned grasp ($COG = (0.5, 0.96)$, $\theta = 0$). (b) Two objects that have a similar plan: the one on the left because it is shifted towards module 1 ($COG = (0.5, 1.18, 0)$, $\theta = 0$), the one on the right (54 g) because it is heavier in correspondence to module 1 ($COG = (0.5, 1.21)$, $\theta = 0$).

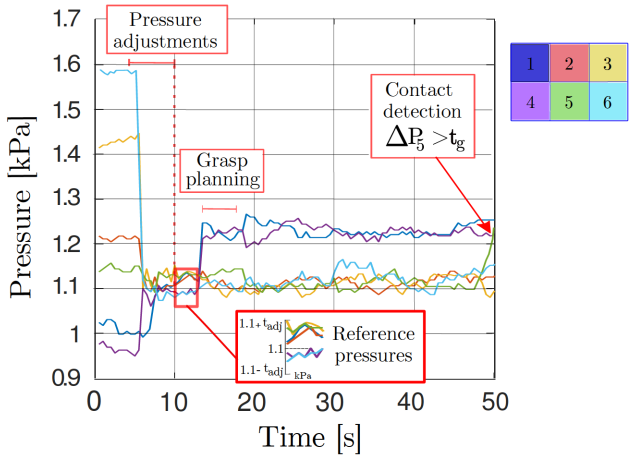

Figure 6.8: Measured pressures during the grasping task with a simple object laying on two adjacent modules (1 and 4). After the reference pressures data saving, the object is placed over the SoftPad and the consequent variations of pressure are registered by the sensors. Having reliable data for the initial reference pressures and the pressures recorded after placing the object over the SoftPad is fundamental. Thus, after the pressure adjustments phase and at the beginning of the grasp planning phase, pressure values are read ten times and the mean values are computed for each module. In this figure, data look noisy mostly because of the pressure sensors performance. While in this work the aim was to demonstrate the feasibility of our approach, in further developments we plan to investigate if changing some parts of the setup we can enhance the accuracy of the grasp planner.

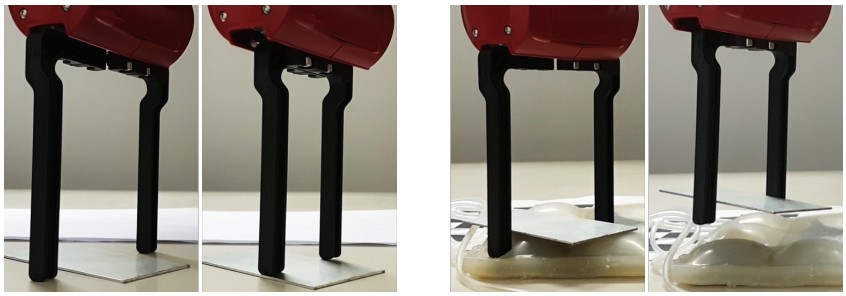

Figure 6.9: A soft environment allows to safely and robustly grasp objects with a rigid gripper. On the left, a case in which it would be impossible for the gripper to grasp the object. On the right, the SoftPad allows the gripper to safely grasp the same object.

grasps that would be impossible for a rigid gripper over a rigid surface due for example to the particular shape of the objects, e.g., flat objects.

Experiment 2: SoftPad aided grasping of a variety of objects

We chose 11 different objects to show the potentialities of the grasp planning algorithm based on the SoftPad pressure readings. During the experimental trials, the robot approached the object with a velocity of 0.05 m/s and each object was grasped and held for 15 s. For each object, we performed five trials. The number of trials was considered appropriate to evaluate the success rate of the experiment: since a rigid gripper, commanded with a velocity controller, is used, the grasp of the object is highly repeatable once the right center and direction of grasp are computed. Thus, the success of the grasp experiment is mostly related to the accuracy of the position and orientation references sent to the robot and these parameters are the output of our grasp planner, which had been also tested in the aforementioned preliminary experiment.

The planned center and direction of grasp obtained in one representative trial are depicted in Fig. 6.10 and reported in Table 6.1, where also objects' weights and success rate in the five trials are listed. An overall success rate of 94.5% was obtained. Objects 1, 2, 3, and 6 are symmetric and with homogeneous weight, thus they were grasped from the middle. For objects 4 and 5, and for the charger, the center of grasp is clearly placed closer to the heaviest part of the object. The cylinder touches all the six modules, so it is seen as a huge rectangle and the direction of grasp is perpendicular to the

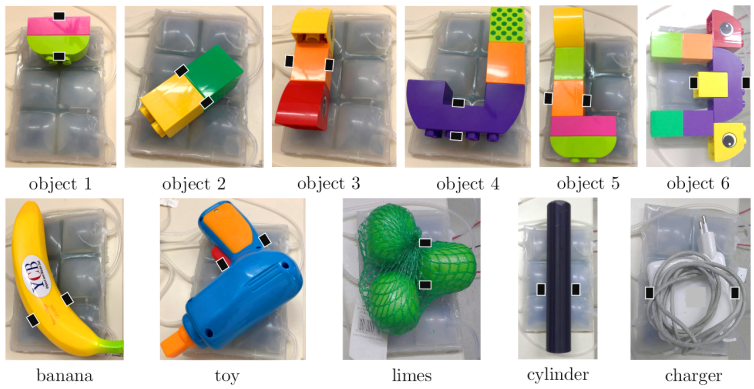

Figure 6.10: Objects used in Experiment 2. The black rectangles indicate the planned position of the fingertips of the gripper.

horizontal axis of the whole SoftPad, i.e., it is $\pi/2$. The cylinder was filled with a heavy small part in one side, that is why the grasp center is not placed exactly in the middle of it. For the banana and the toy, the algorithm worked as in the case of 3-modules objects (Fig. 6.4d-(5) and Fig. 6.4d-(4), respectively), while the limes were considered a 4-modules object (Fig. 6.4e-(2)). In particular, the banana can be considered in the case depicted in Fig. 6.4d-(5) because it lays on modules 2, 3, and 4. Since the COG is in (1, 1), the "major axis" we referred to in Section 6.2 is the one linking the centers of modules 2 and 4, and the angle is $-\pi/4$.

In most of the cases (objects 1, 2, 3, 4, 6, banana, toy, and limes) the grasp was successful five times out of five. Three failures were experienced. Two (object 5, charger) were due to a missing contact detection, because the gripper touched the non-sensitive line between modules. This depends on the size of the gripper tips, which is very small for the chosen gripper. The cylinder was not successfully grasped in one case because the COG was not successfully detected, even if the angle of grasp was correct. It was randomly placed in the middle of the SoftPad similarly to Fig. 6.10 and pressure variations were detected only in four modules. Unfortunately, the resulting COG was in (1, 1.5), which was around 1 cm outside of the object. The chosen gripper (maximum width 6 cm and minimum width 2 cm) could not grasp it. Using a gripper with a wider maximum width and the same minimum width, this case would have been successful. We can conclude that most of the issues could be easily overcome using a gripper with thicker tips and larger maximum width.

Table 6.1: Weight, representative planned grasp (center of grasp (COG) and direction of grasp (θ)), and success rate for the objects in Fig. 6.10. The banana and the Lego Duplo pieces are taken from the YCB Dataset [147].

Object	Weight (g)	Planned grasp $(x_{COG}, y_{COG}, \theta)$	Success rate
object 1	23.8	$(2.5, 1, 0)$	5/5
object 2	25.3	$(1.04, 0.96, \pi/4)$	5/5
object 3	44.4	$(1.5, 1.5, \pi/2)$	5/5
object 4	52	$(0.5, 1.2, 0)$	5/5
object 5	64.9	$(1.36, 1.5, \pi/2)$	4/5
object 6	122	$(1.55, 0.5, \pi/2)$	5/5
banana	59.8	$(1, 1, -\pi/4)$	5/5
toy	131.6	$(2, 1, -\pi/4)$	5/5
limes	187	$(1.5, 0.8, 0)$	5/5
cylinder	88.9	$(1.14, 1, \pi/2)$	4/5
charger	312.3	$(1.16, 1, \pi/2)$	4/5

It is worth noticing that, when using rigid grippers, the inclination of the object may represent an issue. Despite this, during the grasping experiments we carried out we did not experience any failures due to the inclination of the objects. When the gripper closes, its tips slide over the SoftPad and reorient the object. This is one of the advantages of exploiting environmental constraints: the gripper can cope with object pose uncertainties. Note that also the cylinder can be considered an "inclined" object as it is true that it is placed in order and it can easily stand still over the SoftPad, but it touches all modules from the side, generating small pressure variations that sometimes might not be detected.

6.4 Discussion

Even if during the experiments there was no compliance at the tip of the gripper, and thus the interaction between the gripper and the object was still not completely safe, experimental results demonstrated that the intrinsic compliance of the SoftPad can help

in assuring the grasp and in improving safety. Note that in the performed experiments the tips of the gripper were not equipped with soft parts, as for example in [148], because we wanted to evaluate the advantages brought in by the compliance of the SoftPad. Indeed, it is possible to add soft tips to the fingers, but it is a different approach that needs custom design for the gripper and might change the behavior of the gripper itself.

Regarding the working principle of the algorithm, we are aware of the limitations of making assumptions on the shape of the object. For example, it is not possible to accurately trace the borders of the object. In other words, we cannot distinguish the two cases reported in Fig. 6.4b. Most of the times, this does not affect the grasp success rate. Even if the estimation of the center of grasp relies more on the weight distribution than on the shape, objects are unlikely grasped near the extremities. Instead, if the estimation of the angle of grasp is not precise, the soft environment helps in reorienting the object while the gripper closes. However, the reliability of the estimation of center and angle of grasp could be enhanced increasing the resolution of the SoftPad, i.e., using more modules of smaller size.

Clearly there could be real-world applications where some limitations appear. For example, it is not trivial to scale up the SoftPad algorithm for cases requiring a very high number of modules. However, it is unlikely that in a certain task both a large surface to be covered and a high resolution are needed at the same time. A high resolution may be needed for very small objects, but in this case a large surface is rarely required, thus, a limited number of small modules can be used. In most of real applications, the workspace of the robot is proportional to the size of the objects to be grasped. On the contrary, large surface and high resolution may be both required for big objects with a very strange shape. Since most of the common objects do not fall in this category, a SoftPad with a limited number of pads, whose size depends on the objects, can be used.

Visual information could solve some of the problems that might arise with the SoftPad. Cameras are a widespread and validated solution adopted for object recognition, tracking, and grasping [149]. The SoftPad, however, has two main features that a camera cannot offer. First, it can be used to estimate the object center of mass, which is a fundamental object property to take into account when planning grasps [150]. On the contrary, cameras can only provide information pertaining the shape of the object: the weight distribution within the object cannot be determined. Second, the SoftPad senses the interaction between the gripper and the object/environment, which is usually performed by using force/torque sensors at the wrist [127]. Therefore, using the SoftPad we can gather more details useful to safely plan the grasp and we can define a grasping strategy exploitable in cases where it is not possible to use cameras. Besides, with the SoftPad, there is no need of taking into account occlusions, view changes, bad lightning conditions, which

are problems that are commonly encountered with vision systems [151]. However, if it is possible to use cameras, we can surely combine the SoftPad with a vision system and merge the information gathered by the two systems, so to ensure more robust and informative object detection through sensor fusion techniques and obtain a better grasping plan.

6.5 Conclusions

In this chapter, we propose to exploit soft inclusions in the environment to perform robust grasps with rigid grippers. This is achieved through a grasping strategy that uses a sensorized soft layer, called SoftPad, to estimate object pose, shape, and center of mass. To combine the precision of rigid hands with the adaptability of soft hands, we propose to add compliance to the environment and not to the gripper. The main idea behind the development of the SoftPad is that soft sensing modules can be added to the environment to detect $i)$ the contact between the gripper and the environment during grasp approach, and $ii)$ the approximate location and weight distribution of the object to be grasped. Indeed, the great advantage of using the SoftPad as an object pose detector, with respect to having a vision system, is the possibility to estimate the weight distribution. Besides, the same device can be employed to sense the contact between the gripper and the SoftPad, thus performing the role that is usually left to force sensors placed on the hand fingertips or at the robot arm wrist.

The grasp plan computation is based on assumptions that might not be valid for all objects, but, on the one hand, the possibility of sliding over the SoftPad solves possible uncertainties on the object pose, and, on the other hand, the SoftPad parameters (thresholds, inflating pressure) and physical characteristics (size, shape, material) can be changed depending on the application, to be adapted to different sets of objects and requirements. Moreover, parameters can initially be chosen in simulation and then fine tuned with physical experiments.

The possibility of varying the compliance of the modules is considered an important feature of the SoftPad. By changing the value of the inflating pressure it is possible to change the compliance of the SoftPad according to the set of objects that must be grasped. A highly compliant SoftPad detects lighter objects that generate variations of pressure which would not be detected by more rigid modules. For heavy objects, modules inflated at a low pressure would collapse, hence, it is preferable to use considerably higher inflating pressures. In this work, we mainly focused on proving the effectiveness of adding a sensorized soft layer to exploit environmental constraints and detect the mass distribution of the object to be grasped. Thus, we selected an intermediate value

of inflating pressure, which was suitable for all the objects in the set chosen for the experiments. One of the objectives of future developments will be to exploit more the adaptable compliance of the device.

The SoftPad concept is a first step towards the instrumentation of the environment with soft inclusions for exploiting extrinsic, adaptable compliance during grasping and manipulation tasks performed by rigid grippers. A similar device could be, for example, integrated inside a conveyor belt in a factory, or even placed over more complex surfaces thanks to its intrinsic compliance.

Chapter 7
Modeling soft sensorized surfaces: design aspects

Soft robots are spreading quickly and widely thanks to their adaptability, tolerance to uncertainties, reliability, and intrinsic safety. To predict their behaviour, i.e., their final configuration after the interaction with other objects, and to optimize their design, it is fundamental to devise models that account for the fact that they are made of highly non-linear materials and can be subjected to large, continuous deformations.

Well established modeling tools are available for robots composed of rigid links, joints, and actuators: they have a well defined number of degrees of freedom, and classical mechanics methods can be used to describe their dynamics and to properly define their control systems. Soft robots, instead, have structures that can undergo large, continuous deformations, and are made of materials having a non-linear behaviour. Modeling tools for these kinds of devices are less exploited and more complex to manage. Having efficient and accurate models for soft robots, however, is very important in the mechanical design phase and to define proper planning and control strategies. When the focus is on fast simulation and testing of planning and control strategies, it is useful to have computationally efficient models. In [152], for example, a representation based on Cosserat continuous beam theory was used to model compliant joints in underactuated robotic fingers, whereas in [153] results from FEM simulations were employed to develop equivalent lumped parameter models of soft hands with pneumatic actuation.

In this chapter, we focus on modeling the SoftPad, the pneumatically actuated soft robotic device presented in Chapter 6 and developed to provide controllable compliance and sensing capabilities to the environment during grasping tasks with rigid robotic grippers. We concentrate on design aspects, relying on accurate Finite Element Analysis (FEA).

7.1 Modeling the SoftPad

As detailed in Chapter 6, the SoftPad is a modular pneumatic surface made of silicone, which, as well as most of the materials adopted in soft robotics, presents a non-linear, viscoelastic behaviour. Following a procedure similar to [154, 155, 156], we tested differ-

ent non-linear material models to understand which one is more suitable for describing the functioning of the SoftPad. In particular, different models for non-linear materials in FEM static simulations have been tested to evaluate which type of representation is more convenient in terms of accuracy.

Here, we investigate how to model a single module of the SoftPad, but the achieved results could be easily applied to the simulation of the entire device, thanks to its modularity, or to the simulation of pads with different shapes and dimensions.

7.1.1 Models

The most evident difference between linear elastic materials studied in classical structural mechanics and soft materials is that for these ones all the measures, such as stresses and strains, defined for infinitesimal deformations have to be redefined for large, or finite, deformations. Considering a generic isotropic hyperelastic body, in the following, we indicate with $\lambda_1,\ \lambda_2,\ \lambda_3$ the principal stretch ratios, and with I_1, I_2, I_3 the three stretch invariants defined as

$$I_1 = \lambda_1^2 + \lambda_2^2 + \lambda_3^2 \tag{7.1}$$

$$I_2 = \lambda_1^2\lambda_2^2 + \lambda_2^2\lambda_3^2 + \lambda_1^2\lambda_3^2 \tag{7.2}$$

$$I_3 = \lambda_1^2\lambda_2^2\lambda_3^2. \tag{7.3}$$

Hyperelastic or viscoelastic materials in numerical simulations are represented by different non-linear material models. In general, the stress-strain relationship of non-linear materials is represented by means of the strain energy potential W, that can be either a function of the principal stretch ratios or a function of the strain invariants written in Eq. (7.1), Eq. (7.2), and Eq. (7.3).

Non-linear models that can be applied to materials employed in soft robotics include neo-Hookean [157], Mooney-Rivlin [158], Ogden [159], Varga [160], Yeoh [161], and Gent [162]. Viscoelastic models include also time-dependent response due to relaxation or creep phenomena in addition to the non-linear elastic response. Examples of viscoelastic models are Maxwell and Voigt [163]. Here we focus on the steady state response of the SoftPad and thus we do not consider viscoelastic phenomena.

In the following, the main features of the hyperelastic material models employed in our numerical simulations (discussed in Section 7.2) are summarized. A SoftPad made of EcoFlex 00-30 silicone (Smooth-On Inc., USA) was considered. The material parameters' values for each model are reported in Table 7.1. Since in [164] the results obtained studying the mechanical responses of Ecoflex silicone rubber were similar for Ogden and Gent, we chose to test only the first of the two models.

Neo-Hookean model. The strain energy density function for an incompressible neo-Hookean material in a three-dimensional description is defined as

$$W = C_{nh}(I_1 - 3),$$

where the constant C_{nh} is related to the shear modulus μ so that $C_{nh} = \mu/2$.

Mooney-Rivlin model. In the incompressible Mooney-Rivlin model, the strain energy is defined as a function of the invariants I_1 and I_2:

$$W = C_{1mr}(I_1 - 3) + C_{2mr}(I_2 - 3).$$

C_{1mr} and C_{2mr} are constant values depending on material properties that we related to the shear modulus, so that $\mu = 2(C_{1mr} + C_{2mr})$. Their values have to be chosen on the basis of experimental data.

Ogden model. In the Ogden formulation for incompressible materials, the strain energy is expressed as a function of the principal stretch ratios, i.e.,

$$W = \sum_{i=1}^{3} \frac{\mu_i}{\alpha_i} \left({\lambda_1}^{\alpha_i} + {\lambda_2}^{\alpha_i} + {\lambda_3}^{\alpha_i} - 3 \right),$$

where α_i and μ_i are coefficients depending on material properties.

Varga model. Also in the Varga model for incompressible materials the strain energy is defined as a function of principal stretch ratios:

$$W = C_{1v} \left(\lambda_1 + \lambda_2 + \lambda_3 - 3 \right) + C_{2v} \left(\lambda_1\lambda_2 + \lambda_2\lambda_3 + \lambda_1\lambda_3 - 3 \right).$$

In this work, the model coefficients were chosen as: $C_{1v} = 2\mu$ and $C_{2v} = 0$.

Yeoh model. Lastly, in the Yeoh model for incompressible materials, the strain energy is defined as

$$W = C_{1y}(I_1 - 3) + C_{2y}(I_1 - 3)^2 + C_{3y}(I_1 - 3)^3,$$

where C_{1y}, C_{2y} and C_{3y} are coefficients depending on material properties.

In this thesis, for the sake of accuracy we used the nearly incompressible versions of these models. The strain energy density in this case is composed of two terms: $W = W_{iso} + W_{vol}$ [165]. W_{iso} represents the isochoric part and has the same expression

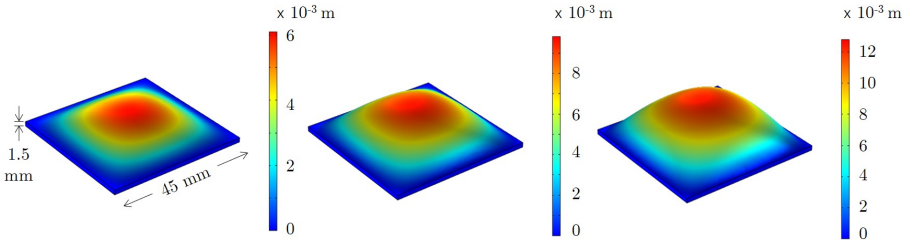

Figure 7.1: Module deformation for neo-Hookean material at pressures $\{0.5, 1.5, 2.5\}$ kPa.

of the strain energy density defined above for the incompressible case, but I_1, I_2, and λ_i are substituted, respectively, with[1]

$$\bar{I}_1 = J_{el}^{-\frac{2}{3}} I_1, \quad \bar{I}_2 = J_{el}^{-\frac{4}{3}} I_2, \quad \bar{\lambda_i} = J_{el}^{-\frac{1}{3}} \lambda_i,$$

where J_{el} is the elastic volume ratio. W_{vol} is the volumetric strain energy that is expressed as: $\frac{1}{2}\kappa(J_{el}-1)^2$, where κ is the initial bulk modulus. We chose $\kappa = 10^5\mu$.

7.2 Simulations

After creating a FEM model of a single module of the SoftPad, a set of simulations with different material models were conducted. Fig. 7.1 shows an example of obtained deformations using the neo-Hookean model. As FE simulator we used COMSOL Multiphysics 5.4 (Comsol Inc., USA). The Nonlinear Structural Materials Module of Comsol provides several predefined material models together with an option to enter user defined expressions for the strain energy density.

The simulated module was a 45×45×1.5 mm block. On the lateral faces, a fixed constraint was applied, while a uniform pressure was applied to the lower surface. The coefficients for Ecoflex 00-30 silicone rubber models that were employed for the simulations were derived from [166, 164, 167].

[1] Note that COMSOL considers the principal stretches of the elastic deformation, i.e., the principal elastic stretches λ_{eli}, and not the principal stretches of the overall deformation considering also the inelastic part [165]. Here we omit the subscript for brevity.

Table 7.1: Parameters depending on material properties for the models considered in the simulations, relative to EcoFlex 00-30 silicone [166, 164, 167].

Model	Parameters	
Neo Hookean and Varga	Symbol	Value
	μ	42 kPa
Mooney-Rivlin	Symbol	Value
	C_{1mr}	0.4375μ
	C_{2mr}	0.0625μ
Ogden [164]	i α_i	μ_i
	1 1.3	22kPa
	2 5	0.4kPa
	3 -2	-2kPa
Ogden [166]	i α_i	μ_i
	1 1.7138	24.3kPa
	2 7.0679	0.0667kPa
	3 3.3659	0.4538kPa
Yeoh	Symbol	Value
	C_{1y}	17 kPa
	C_{2y}	-0.2 kPa
	C_{3y}	0.023 kPa

In a first set of simulations, we compared the results obtained from FEM simulation in terms of overall deformation of the pad with the mean of some experimental measures that we took on three different modules (as shown in Fig. 7.2a and Fig. 7.2b). An inflating pressure from 0 to 3 kPa was applied and the deformation was estimated as the maximum height of the module, corresponding to its center. Results show that the neo-Hookean model follows quite well the behaviour of the experimental data for

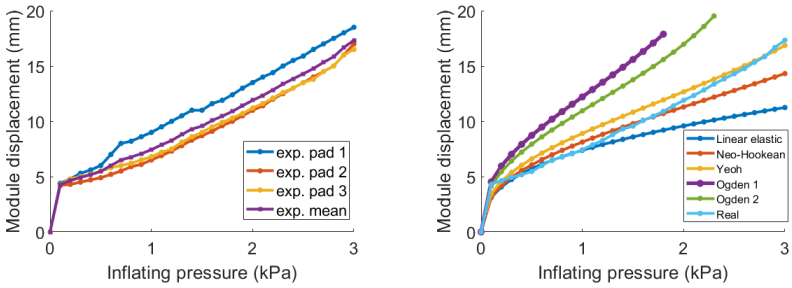

(a) (b)

Figure 7.2: First set of experiments: comparison of different material models. (a) Measured deformations of three different real modules as a function of the inflating pressure; (b) comparison between the mean measured deformation and the deformations predicted with different material models.

small deformations and almost overlaps it in the range [1.4, 1.8] kPa, while the Yeoh model fits better for large deformations. We computed the root mean square error between the mean of the real measurements and the simulated data and we obtained $RMSE_{nh} = 1.1289$ mm and $RMSE_y = 0.9259$ mm for the neo-Hookean and the Yeoh models, respectively. We also tested Mooney-Rivlin and Varga material models. The obtained results had a similar trend to that of the neo-Hookean model, but presented a higher RMSE ($RMSE_{mr}$ =1.2775 mm, $RMSE_v$ =1.2367 mm), thus we did not report them in the diagram for the sake of clarity. The Ogden model largely overestimated the overall deformation with two different sets of coefficients found in [164] for Ogden 1 and in [166] for Ogden 2. Probably, in this case, an ad hoc parameter estimation should be carried out in order to have a better fit.

In a second set of experiments we took the best two models (i.e., neo-Hookean and Yeoh) and considered how the deformation of a module varies with respect to two construction parameters: the height of the upper layer and the width of the module of the SoftPad. During the simulations, the inflating pressure was set to 1 kPa. Fig. 7.3a shows that the thicker is the layer, the lower is the produced deformation. The contrary happens with respect to the module width (see Fig. 7.3b): the larger is the module, the more it deforms, once the inflating pressure is fixed. As above, the Yeoh model shows a higher deformation with respect to the neo-Hookean.

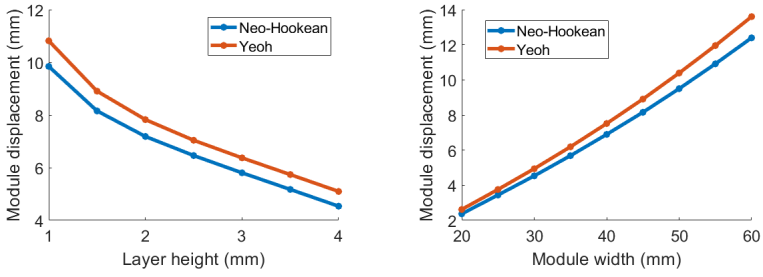

(a) (b)

Figure 7.3: Second set of experiments: module maximum displacement (a) with respect to the height of the upper layer and (b) with respect to the width of a module of the SoftPad. Data are gathered simulating an inflating pressure of 1 kPa.

7.3 Conclusions

In this chapter, we addressed the problem of finding an accurate model of a pneumatic module that we developed for the soft sensorized device called SoftPad. Different models of non-linear materials available in the literature were compared in terms of accuracy in reproducing the deformation of the module when an inflating pressure is applied to it. By comparing the simulation results with measured deformations of three modules with the same nominal dimensions, we observed that both the neo-Hookean and the Yeoh models are able to describe the device behavior with a sufficiently good approximation. In particular, Yeoh model fits better for large deformations.

A reliable simulation model of this type of components is useful in the design phase, since it can be employed to predict the relationship between pressure and deformation as a function of the main design parameters. In this thesis, we focused on a device with a relatively simple geometrical shape, but we believe that the results of this study can be extended to more complex structures, as for instance soft robotic hands made of silicone rubber [125].

Conclusions and future work

This thesis presents my contribution to the field of robotics and haptics, collecting all the work I have done from October 2017 to September 2020 toward my Ph.D. degree.

In these years, first, I tried to contribute to address the challenge of increasing safety during surgical procedures, by measuring contact forces occurring during the interaction between instruments and anatomical areas. Although haptic perception is of primary importance while performing surgery, in robotic minimally invasive surgery the surgeon can rely only on visual feedback and, besides, there could be also procedures in open surgery in which a reduction of tactile perception may occur. For this reason, restoring the sense of touch is an emerging need several researchers tried to address. To this aim, in this thesis I focused on surgical instruments, proposing different novel pneumatic methods to estimate contact forces both in robotic and open surgery. The collected results paved the way towards the exploitation of novel pneumatic-based devices for contact detection in more general scenarios. For example, a pneumatic device has been proposed to create soft inclusions in the environment that can be used by rigid grippers to achieve safer grasps.

The motivation which led to these works is clearly stated in Chapter 1, where also the state of the art of force sensing in surgical frameworks is discussed. It is well-known that haptic feedback can complement other sensory modalities and for instance counterbalance the narrow camera view available in minimally invasive surgery. Among the several applications present in the literature, robot-assisted palpation seems to be particularly favored by the addition of haptic signals and without them excessive forces might be applied by the surgeon causing complications.

Chapter 2 introduces the design of a novel pneumatic force sensor for robot-assisted surgery, that takes advantage of measuring pressure variations inside a pneumatic balloon to estimate the interaction force between surgical tools and patient's tissues. This chapter

is based on the work published as [168]. In this work, an elastic and sphere-shaped membrane is placed in a tiny hollow inside the surgical instrument, very close to the tip. By inflating this pneumatic balloon, it goes out from its cavity only when force measurement is required. Once it comes into contact with the human tissue, a change in the air pressure inside the balloon is registered by a pressure sensor: this value is proportional to the norm of the contact force. In a first approach, the relationship between contact force and pressure variation has been experimentally detected. The effectiveness of the pressure based method has been confirmed by experimental results.

This innovative approach has been recalled in Chapter 3 with the aim of better investigating the relationship between the norm of the contact force and the subsequent variation of pressure inside the membrane. This chapter is a revised version of the work published as [169] and presents a mathematical model relating the intensity of the contact force to the variation of pressure, based on geometrical considerations combined with an energetic approach. The mathematical model was validated through experiments whose results showed agreement between model predicted data and ground-truth values measured by a commercial force sensor. The promising results demonstrates the method reliability despite its simple and intuitive technology.

The pneumatic approach is considered beneficial in several ways. Primarily, the use of disposable materials already widespread in surgery, such as latex, polyurethane, or silicone, avoids sterilization and biocompatibility issues. The location of the pneumatic sensor represents an additional benefit: it is hidden inside the body of the instrument when force measurement is not needed, so it does not limit the surgical workspace during the standard medical procedures. Only after inflation, it comes out from its housing in the proximity of the tip of the instrument, enabling the surgeon to palpate the tissue of interest. Another fundamental aspect is cost reduction: since most of the surgical tools in RMIS are disposable because of sterilizability reasons, the sensing system must not represent a significant cost. Our device complies with this requirement because the pressure sensor and the electronics can be located out of the operational workspace and do not have to be replaced after every operation. Indeed, the only part that enters the human body is the membrane and measurement information is transferred by means of a gas to the sensitive components. Another advantage of the presented device is the possibility to set the inflating pressure so as to have a sensor with different stiffnesses depending on the anatomical area.

Although this pneumatic sensor has been developed for force evaluation during RMIS procedures and thus its features (e.g., small size, lightweight, biocompatibility, etc.) have been specifically designed to solve issues related to robotic surgery, the obtained results may be suitable for any master-slave technology. For example, the sensing principle

of the pneumatic device and its beneficial features (e.g., the possibility of tuning the stiffness) can be advantageously used to estimate contact forces occurring in several remote manipulation tasks, integrating one or more pneumatic balloons in a robotic hand.

The initial prototype size is still far from the surgery application requirements, but it was suitable for a preliminary method validation with promising results. Further developments will be focused on the miniaturization of the sensing device, possible due to its simple structure, and on the actual integration with surgical tools. Surgeons' opinion on how to improve device ergonomics will be asked and feasibility in practical usage will be explored. After miniaturization, the sensor will be properly characterized evaluating its force range and resolution at different pressure values. Also a different set of elastic biocompatible materials will be tested to understand which one might be the best for different specific surgical tasks. In future works, also the stiffness measurement carried out by a pair of pneumatic balloons and the force estimation method based on vision will be extensively investigated. Among the different application scenarios that will be explored, the integration of pneumatic balloons in a robotic hand will demand particular attention.

Regarding the mathematical model, future development will also consider using other techniques, for example based on vision, to estimate the initial radius of the membrane.

In Chapter 4, a novel pneumatic device to estimate contact forces between hand-held surgical drills and bones has been presented. This chapter is an extended version of the work published as [170]. With respect to the previous works, this device has been specifically developed for surgical drills used in open surgery. It consists in a cover equipped with soft silicone pipes representing the sensing element. The contact forces are estimated by means of the variation of pressure which occurs inside one or more pipes, depending on the direction of the force. In addition to the innovative working principle, another novelty of this work is that the device has been not only validated in comparison with a commercial force sensor, but also tested in combination with a haptic display for force feedback in a preliminary experimental campaign. Also in this case, the use of a gas as a means to estimate interaction forces represents a major advantage in terms of delocalization of the electronics, size, cost, and biocompatibility. The development of a more ergonomic cover is planned for next works, together with a more accurate haptic display, and the investigation on the best location and type of feedback. Additional metrics, such as tissue discrimination, will be considered to evaluate the accuracy of the device and of the type of feedback. Several tests with tissues of different consistencies will be conducted. Learning curves in performing the task with and without feedback will be evaluated in a more careful future study, involving a larger sample. Further studies will be conducted considering also the participants emotional state and the cognitive load

during the performance with and without haptic feedback.

The results presented in the first chapters of this thesis paved the way for a new interesting research line focused on pneumatic-based methods exploited not only for force sensing in surgery, but also for a more general contact detection in a wide range of applications. This research direction has been further explored in Chapter 5, Chapter 6, and Chapter 7. Chapter 5 makes an introduction on soft robotics and presents the concept of a soft modular pneumatic surface, called the SoftPad. In Chapter 6 an exhaustive explanation of the SoftPad features is provided. These chapters are based on a revised version of the work published as [171].

The SoftPad has been developed to add compliance to the environment during grasping tasks, thus improving the grasp performance in terms of robustness to uncertainties, and to detect object features and contact events. It consists of a matrix of silicone pneumatic modules, whose number, geometrical properties, and arrangement can be adapted to the specific context. Each module is connected to a pressure sensor and the contact between the SoftPad and an object placed over it can be detected by reading pressure variations in the modules. Thanks to the grasp planning algorithm that was devised in this work, the SoftPad can be used to plan grasps in situations where cameras are not available, or where object mass distribution estimation is paramount and cannot be done a priori, supporting or even substituting other types of sensors typically needed in grasping, like vision systems.

With respect to the pneumatic devices presented in the previous chapters, here a similar reasoning has been exploited, but the variation of pressure sensed in the modules of the SoftPad has been used to detect events related to the grasping task. Depending on the entity of the variation and on the involved modules, object pose, approximate shape, and center of mass can be estimated. This information can be used as an input for the grasp planner of a robot equipped with a rigid gripper. As well as the pneumatic balloon, the SoftPad brings in the advantages of soft robots, and in particular the possibility of having a device that has sensing capabilities and at the same time ensures a safe interaction between the robot and the environment.

The use of pressure sensors allows to delocalize the electronics, ensuring a high-temperature resistant and washable device in the work-space, and to change the compliance of the modules according to the objects to grasp. One of the objectives of future developments will be to exploit more the adaptable compliance of the device. The possibility of varying the inflating pressure may be exploited also to adapt the compliance of the SoftPad to the approaching velocity of the robot, to ensure a safe and stable impact even in case of high robot velocities.

The SoftPad can be used to grasp objects with sizes, weights and shapes varying in

quite wide ranges, by easily adapting the design. In future work we target to improve the grasping algorithm in terms of scalability to make it capable of working with potentially any number of soft modules. We will also advance the simulation framework, to achieve a platform for iterative design of the SoftPad based on gripper and objects properties. The possibility of accurately modeling the behavior of the SoftPad will allow us to evaluate the interplay between different parameters (size, material, inflating pressure, etc.) in simulation before actually building the prototype, thus leading to an efficient process of iterative design.

Regarding the last point, in Chapter 7 the behavior of the SoftPad has been studied through Finite Element Analysis (FEA) and several material models have been tested to understand which one is most suitable for describing the functioning of a single module. Results shows that both the neo-Hookean and the Yeoh models describe the behavior of a SoftPad module with a sufficiently good approximation. Future research on this topic will include a deeper analysis of material properties, the evaluation of other structural properties of the modules, and the contact and interaction problem between the compliant surface of the module and a rigid object. Chapter 7 is a revised version of the work published as [172].

Bibliography

[1] D. Keltner, "Hands on research: The science of touch," *Greater Good Magazine*, September 29, 2010.

[2] K. Barnett, "A theoretical construct of the concepts of touch as they relate to nursing," *Nursing Research*, vol. 21, no. 2, pp. 102–109, 1972.

[3] F. A. Geldard, "Some neglected possibilities of communication," *Science*, vol. 131, no. 3413, pp. 1583–1588, 1960.

[4] T. M. Field, S. M. Schanberg, F. Scafidi, C. R. Bauer, N. Vega-Lahr, R. Garcia, J. Nystrom, and C. M. Kuhn, "Tactile/kinesthetic stimulation effects on preterm neonates," *Pediatrics*, vol. 77, no. 5, pp. 654–658, 1986.

[5] P. Hawranik, P. Johnston, and J. Deatrich, "Therapeutic touch and agitation in individuals with Alzheimer's disease," *Western journal of nursing research*, vol. 30, no. 4, pp. 417–434, 2008.

[6] M. Ashfeld, "Effect of therapeutic touch in treating agitation of persons with Alzheimer's disease," 2011.

[7] E. Kim and M. Buschmann, "The effect of expressive physical touch on patients with dementia," *International Journal of Nursing Studies*, vol. 36, no. 3, pp. 235–243, 1999.

[8] D. Nelson, "The power of human touch in Alzheimer's care," *Massage Therapy Journal*, vol. 43, pp. 82–92, 2004.

[9] R. I. Dunbar, "The social role of touch in humans and primates: behavioural function and neurobiological mechanisms," *Neuroscience & Biobehavioral Reviews*, vol. 34, no. 2, pp. 260–268, 2010.

[10] J. K. Burgoon, J. B. Walther, and E. J. Baesler, "Interpretations, evaluations, and consequences of interpersonal touch," *Human Communication Research*, vol. 19, no. 2, pp. 237–263, 1992.

[11] M. A. Srinivasan and C. Basdogan, "Haptics in virtual environments: Taxonomy, research status, and challenges," *Computers & Graphics*, vol. 21, no. 4, pp. 393–404, 1997.

[12] A. M. Okamura, "Haptic feedback in robot-assisted minimally invasive surgery," *Current opinion in urology*, vol. 19, no. 1, pp. 102–107, 2009.

[13] J. Hergenhan, J. Rutschke, M. Uhl, S. E. Navarro, B. Hein, and H. Worn, "A haptic display for tactile and kinesthetic feedback in a CHAI 3D palpation training scenario," in *Proceedings of IEEE International Conference on Robotics and Biomimetics (ROBIO)*, pp. 291–296, 2015.

[14] J. Chen, M. Holbein, and J. S. Zelek, "Intro to haptic communications for high school students," in *Proceedings of IEEE International Conference on Robotics and Automation*, pp. 733–738, 2006.

[15] M. V. Ottermo, M. Øvstedal, T. Langø, Ø. Stavdahl, Y. Yavuz, T. A. Johansen, and R. Mårvik, "The role of tactile feedback in laparoscopic surgery," *Surgical Laparoscopy Endoscopy & Percutaneous Techniques*, vol. 16, no. 6, pp. 390–400, 2006.

[16] H. C. Bastian, *The brain as an organ of mind*. D. Appleton and Company, 1883.

[17] L. A. Jones, "Kinesthetic sensing," in *Human and Machine Haptics*, MIT Press, 2000.

[18] B. B. Edin and N. Johansson, "Skin strain patterns provide kinaesthetic information to the human central nervous system," *The Journal of physiology*, vol. 487, no. 1, pp. 243–251, 1995.

[19] W. R. Ferrell, S. C. Gandevia, and D. I. McCloskey, "The role of joint receptors in human kinaesthesia when intramuscular receptors cannot contribute," *The Journal of physiology*, vol. 386, pp. 63–71, 1987.

[20] F. J. Clark, R. C. Burgess, and J. W. Chapin, "Proprioception with the proximal interphalangeal joint of the index finger," *Brain*, vol. 109, no. 6, pp. 1195–1208, 1986.

[21] F. J. Clark, K. W. Horch, S. M. Bach, and G. F. Larson, "Contributions of cutaneous and joint receptors to static knee-position sense in man," *Journal of Neurophysiology*, vol. 42, no. 3, pp. 877–888, 1979.

[22] V. E. Abraira and D. D. Ginty, "The sensory neurons of touch," *Neuron*, vol. 79, no. 4, pp. 618–639, 2013.

[23] L. A. Jones and A. M. Smith, "Tactile sensory system: encoding from the periphery to the cortex," *Wiley Interdisciplinary Reviews: Systems Biology and Medicine*, vol. 6, no. 3, pp. 279–287, 2014.

[24] C. F. Bolton, R. K. Winkelmann, and P. J. Dyck, "A quantitative study of Meissner's corpuscles in man," *Neurology*, vol. 16, no. 1, pp. 1–9, 1966.

[25] J. P. Lacour, D. Dubois, A. Pisani, and J. P. Ortonne, "Anatomical mapping of Merkel cells in normal human adult epidermis," *British Journal of Dermatology*, vol. 125, no. 6, pp. 535–542, 1991.

[26] M. Paré, C. Behets, and O. Cornu, "Paucity of presumptive Ruffini corpuscles in the index finger pad of humans," *Journal of Comparative Neurology*, vol. 456, no. 3, pp. 260–266, 2003.

[27] J. Bell, S. Bolanowski, and M. H. Holmes, "The structure and function of Pacinian corpuscles: a review," *Progress in neurobiology*, vol. 42, no. 1, pp. 79–128, 1994.

[28] R. D. Howe, "Tactile sensing and control of robotic manipulation," *Advanced Robotics*, vol. 8, no. 3, pp. 245–261, 1993.

[29] C. Bartolozzi, L. Natale, F. Nori, and G. Metta, "Robots with a sense of touch," *Nature materials*, vol. 15, no. 9, p. 921, 2016.

[30] T. B. Sheridan, "Teleoperation, telerobotics and telepresence: A progress report," *Control Engineering Practice*, vol. 3, no. 2, pp. 205–214, 1995.

[31] H. Das, H. Zak, W. S. Kim, A. K. Bejczy, and P. S. Schenker, "Operator performance with alternative manual control modes in teleoperation," *Presence: Teleoperators & Virtual Environments*, vol. 1, no. 2, pp. 201–218, 1992.

[32] T. B. Sheridan, *Telerobotics, automation, and human supervisory control*. MIT press, 1992.

[33] N. Durlach and M. Slater, "Presence in shared virtual environments and virtual togetherness," *Presence: Teleoperators & Virtual Environments*, vol. 9, no. 2, pp. 214–217, 2000.

[34] M. J. Massimino and T. B. Sheridan, "Teleoperator performance with varying force and visual feedback," *Human Factors: The Journal of the Human Factors and Ergonomics Society*, vol. 36, no. 1, pp. 145–157, 1994.

[35] L. Moody, C. Baber, T. N. Arvanitis, *et al.*, "Objective surgical performance evaluation based on haptic feedback," *Studies in health technology and informatics*, pp. 304–310, 2002.

[36] C. Pacchierotti, F. Chinello, M. Malvezzi, L. Meli, and D. Prattichizzo, "Two finger grasping simulation with cutaneous and kinesthetic force feedback," in *Proceedings of International Conference on Human Haptic Sensing and Touch Enabled Computer Applications*, pp. 373–382, 2012.

[37] B. Hannaford, "Task-level testing of the JPL-OMV smart end effector," in *Proceedings of the Workshop on Space Telerobotics*, vol. 2, 1987.

[38] C. R. Wagner, N. Stylopoulos, and R. D. Howe, "The role of force feedback in surgery: analysis of blunt dissection," in *Proceedings of IEEE International Symposium on Haptic Interfaces for Virtual Environment and Teleoperator Systems*, pp. 68–74, 2002.

[39] S. E. Salcudean, S. Ku, and G. Bell, "Performance measurement in scaled teleoperation for microsurgery," in *Proceedings of the First Joint Conference on Computer Vision, Virtual Reality and Robotics in Medicine and Medial Robotics and Computer-Assisted Surgery*, pp. 789–798, 1997.

[40] M. Abayazid, C. Pacchierotti, P. Moreira, R. Alterovitz, D. Prattichizzo, and S. Misra, "Experimental evaluation of co-manipulated ultrasound-guided flexible needle steering," *The International Journal of Medical Robotics and Computer Assisted Surgery*, vol. 12, no. 2, pp. 219–230, 2016.

[41] A. Kazi, "Operator performance in surgical telemanipulation," *Presence: Teleoperators & Virtual Environments*, vol. 10, no. 5, pp. 495–510, 2001.

[42] C. Pacchierotti, D. Prattichizzo, and K. J. Kuchenbecker, "Cutaneous feedback of fingertip deformation and vibration for palpation in robotic surgery," *IEEE Transactions on Biomedical Engineering*, vol. 63, no. 2, pp. 278–287, 2016.

[43] C. W. Kennedy, T. Hu, J. P. Desai, A. S. Wechsler, and J. Y. Kresh, "A novel approach to robotic cardiac surgery using haptics and vision," *Cardiovascular Engineering*, vol. 2, no. 1, pp. 15–22, 2002.

[44] D. De Lorenzo, E. De Momi, I. Dyagilev, R. Manganelli, A. Formaglio, D. Prattichizzo, M. Shoham, and G. Ferrigno, "Force feedback in a piezoelectric linear actuator for neurosurgery," *The International Journal of Medical Robotics and Computer Assisted Surgery*, vol. 7, no. 3, pp. 268–275, 2011.

[45] M. Tavakoli, R. Patel, and M. Moallem, "Haptic interaction in robot-assisted endoscopic surgery: a sensorized end-effector," *The International Journal of Medical Robotics and Computer Assisted Surgery*, vol. 1, no. 2, pp. 53–63, 2005.

[46] A. Pillarisetti, M. Pekarev, A. D. Brooks, and J. P. Desai, "Evaluating the effect of force feedback in cell injection," *IEEE Transactions on Automation Science and Engineering*, vol. 4, no. 3, pp. 322–331, 2007.

[47] E. P. Westebring-Van Der Putten, R. H. M. Goossens, J. J. Jakimowicz, and J. Dankelman, "Haptics in minimally invasive surgery–a review," *Minimally Invasive Therapy & Allied Technologies*, vol. 17, no. 1, pp. 3–16, 2008.

[48] A. R. Lanfranco, A. E. Castellanos, J. P. Desai, and W. C. Meyers, "Robotic surgery: a current perspective," *Annals of surgery*, vol. 239, no. 1, pp. 14–21, 2004.

[49] G. Tholey, J. P. Desai, and A. E. Castellanos, "Force feedback plays a significant role in minimally invasive surgery: results and analysis," *Annals of surgery*, vol. 241, no. 1, p. 102, 2005.

[50] M. Van Veelen, E. Nederlof, R. Goossens, C. Schot, and J. Jakimowicz, "Ergonomic problems encountered by the medical team related to products used for minimally invasive surgery," *Surgical Endoscopy and Other Interventional Techniques*, vol. 17, no. 7, pp. 1077–1081, 2003.

[51] P. Kornprat, G. Werkgartner, H. Cerwenka, H. Bacher, A. El-Shabrawi, P. Rehak, and H. J. Mischinger, "Prospective study comparing standard and robotically assisted laparoscopic cholecystectomy," *Langenbeck's archives of surgery*, vol. 391, no. 3, pp. 216–221, 2006.

[52] O. A. J. Van der Meijden and M. P. Schijven, "The value of haptic feedback in conventional and robot-assisted minimal invasive surgery and virtual reality training: a current review," *Surgical Endoscopy*, vol. 23, no. 6, pp. 1180–1190, 2009.

[53] A. Faragasso, A. Stilli, J. Bimbo, H. A. Wurdemann, and K. Althoefer, "Multi-axis stiffness sensing device for medical palpation," in *Proceedings of IEEE/RSJ International Conference on Intelligent Robots and Systems (IROS)*, pp. 2711–2716, 2015.

[54] G. De Gersem, H. Van Brussel, and F. Tendick, "Reliable and enhanced stiffness perception in soft-tissue telemanipulation," *The International Journal of Robotics Research*, vol. 24, no. 10, pp. 805–822, 2005.

[55] P. Valdastri, M. Simi, and R. J. Webster III, "Advanced technologies for gastrointestinal endoscopy," *Annual Review of Biomedical Engineering*, vol. 14, pp. 397–429, 2012.

[56] N. R. Ellis, "Handbook of mental deficiency: Psychological theory and research," 1964.

[57] J. M. Godlove, E. O. Whaite, and A. P. Batista, "Comparing temporal aspects of visual, tactile, and microstimulation feedback for motor control," *Journal of Neural Engineering*, vol. 11, no. 4, p. 046025, 2014.

[58] J. D. Brown, J. N. Fernandez, S. P. Cohen, and K. J. Kuchenbecker, "A wrist-squeezing force-feedback system for robotic surgery training," in *Proceedings of IEEE World Haptics Conference (WHC)*, pp. 107–112, 2017.

[59] L. Meli, C. Pacchierotti, and D. Prattichizzo, "Experimental evaluation of magnified haptic feedback for robot-assisted needle insertion and palpation," *The International Journal of Medical Robotics and Computer Assisted Surgery*, vol. 13:e1809, 2017.

[60] M. Mahvash, J. Gwilliam, R. Agarwal, B. Vagvolgyi, L.-M. Su, D. D. Yuh, and A. M. Okamura, "Force-feedback surgical teleoperator: Controller design and palpation experiments," in *Proceedings of IEEE International Symposium in Haptic Interfaces for Virtual Environment and Teleoperator Systems*, pp. 465–471, 2008.

[61] L. Fichera, C. Pacchierotti, E. Olivieri, D. Prattichizzo, and L. S. Mattos, "Kinesthetic and vibrotactile haptic feedback improves the performance of laser microsurgery," in *Proceedings of IEEE Haptics Symposium*, pp. 59–64, 2016.

[62] A. M. Okamura, "Methods for haptic feedback in teleoperated robot-assisted surgery," *Industrial Robot: An International Journal*, vol. 31, no. 6, pp. 499–508, 2004.

[63] A. I. Aviles, S. M. Alsaleh, P. Sobrevilla, and A. Casals, "Force-feedback sensory substitution using supervised recurrent learning for robotic-assisted surgery," in *Proceedings of IEEE International Conference on Engineering in Medicine and Biology Society*, pp. 1–4, 2015.

[64] P. Puangmali, K. Althoefer, L. D. Seneviratne, D. Murphy, and P. Dasgupta, "State-of-the-art in force and tactile sensing for minimally invasive surgery," *IEEE Sensors Journal*, vol. 8, no. 4, pp. 371–381, 2008.

[65] Y. Luo and B. J. Nelson, "Fusing force and vision feedback for manipulating deformable objects," *Journal of Field Robotics*, vol. 18, no. 3, pp. 103–117, 2001.

[66] E. Noohi, S. Parastegari, and M. Žefran, "Using monocular images to estimate interaction forces during minimally invasive surgery," in *Proceedings of IEEE/RSJ International Conference on Intelligent Robots and Systems*, pp. 4297–4302, 2014.

[67] A. I. Aviles, S. Alsaleh, P. Sobrevilla, and A. Casals, "Sensorless force estimation using a neuro-vision-based approach for robotic-assisted surgery," in *Proceedings of IEEE/EMBS International Conference on Neural Engineering*, pp. 86–89, 2015.

[68] T. H. Pham, A. Kheddar, A. Qammaz, and A. Argyros, "Capturing and reproducing hand-object interactions through vision-based force sensing," in *IEEE ICCV Workshop on Object Understanding for Interaction*, 2015.

[69] A. Faragasso, J. Bimbo, Y. Noh, A. Jiang, S. Sareh, H. Liu, T. Nanayakkara, H. A. Wurdemann, and K. Althoefer, "Novel uniaxial force sensor based on visual information for minimally invasive surgery," in *Proceedings of IEEE International Conference on Robotics and Automation*, pp. 1405–1410, 2014.

[70] C. H. King, M. O. Culjat, M. L. Franco, C. E. Lewis, E. P. Dutson, W. S. Grundfest, and J. W. Bisley, "Tactile feedback induces reduced grasping force in robot-assisted surgery," *IEEE Transactions on Haptics*, vol. 2, no. 2, pp. 103–110, 2009.

[71] A. Sarmah and U. Gulhane, "Surgical robot teleoperated laparoscopic grasper with haptics feedback system," in *IEEE INTERACT-2010*, pp. 288–291, 2010.

[72] P. Puangmali, H. Liu, L. D. Seneviratne, P. Dasgupta, and K. Althoefer, "Miniature 3-axis distal force sensor for minimally invasive surgical palpation," *IEEE/ASME Transactions On Mechatronics*, vol. 17, no. 4, pp. 646–656, 2011.

[73] A. Nakai, K. Kuwana, K. Saito, T. Dohi, A. Kumagai, and I. Shimoyama, "MEMS 6-axis force-torque sensor attached to the tip of grasping forceps for identification of tumor in thoracoscopic surgery," in *Proceedings of the IEEE 30th International Conference on Micro Electro Mechanical Systems (MEMS)*, pp. 546–548, 2017.

[74] B. Gonenc, A. Chamani, J. Handa, P. Gehlbach, R. H. Taylor, and I. Iordachita, "3-DOF force-sensing motorized micro-forceps for robot-assisted vitreoretinal surgery," *IEEE Sensors Journal*, vol. 17, no. 11, pp. 3526–3541, 2017.

[75] P. Polygerinos, P. Puangmali, T. Schaeffter, R. Razavi, L. D. Seneviratne, and K. Althoefer, "Novel miniature MRI-compatible fiber-optic force sensor for cardiac catheterization procedures," in *Proceedings of IEEE International Conference on Robotics and Automation*, pp. 2598–2603, 2010.

[76] M. C. Yip, S. G. Yuen, and R. D. Howe, "A robust uniaxial force sensor for minimally invasive surgery," *IEEE Transactions on Biomedical Engineering*, vol. 57, no. 5, pp. 1008–1011, 2010.

[77] N. Wettels, L. M. Smith, V. J. Santos, and G. E. Loeb, "Deformable skin design to enhance response of a biomimetic tactile sensor," in *Proceedings of IEEE International Conference on Biomedical Robotics and Biomechatronics*, pp. 132–137, 2008.

[78] M. Louredo, I. Díaz, and J. J. Gil, "Dribon: A mechatronic bone drilling tool," *Mechatronics*, vol. 22, no. 8, pp. 1060–1066, 2012.

[79] I. Díaz, J. J. Gil, and M. Louredo, "Bone drilling methodology and tool based on position measurements," *Computer methods and programs in biomedicine*, vol. 112, no. 2, pp. 284–292, 2013.

[80] H. Sang, R. Monfaredi, E. Wilson, H. Fooladi, D. Preciado, and K. Cleary, "A new surgical drill instrument with force sensing and force feedback for robotically assisted otologic surgery," *Journal of Medical Devices*, vol. 11, no. 3, 2017.

[81] M. Hessinger, J. Hielscher, P. P. Pott, and R. Werthschützky, "Handheld surgical drill with integrated thrust force recognition," in *Proceedings of IEEE International Conference on E-Health and Bioengineering Conference*, pp. 1–4, 2013.

[82] P. Brett, D. Baker, L. Reyes, and J. Blanshard, "An automatic technique for micro-drilling a stapedotomy in the flexible stapes footplate," *Proceedings of the Institution of Mechanical Engineers, Part H: Journal of Engineering in Medicine*, vol. 209, no. 4, pp. 255–262, 1995.

[83] B. Allotta, G. Giacalone, and L. Rinaldi, "A hand-held drilling tool for orthopedic surgery," *IEEE/ASME Transactions on Mechatronics*, vol. 2, no. 4, pp. 218–229, 1997.

[84] X. Du, M. Z. Assadi, F. Jowitt, P. N. Brett, S. Henshaw, J. Dalton, D. W. Proops, C. J. Coulson, and A. P. Reid, "Robustness analysis of a smart surgical drill for cochleostomy," *The International Journal of Medical Robotics and Computer Assisted Surgery*, vol. 9, no. 1, pp. 119–126, 2013.

[85] F. Ong and K. Bouazza-Marouf, "The detection of drill bit break-through for the enhancement of safety in mechatronic assisted orthopaedic drilling," *Mechatronics*, vol. 9, no. 6, pp. 565–588, 1999.

[86] S. Grange, F. Conti, P. Rouiller, P. Helmer, and C. Baur, "The Delta haptic device," 2001.

[87] T. H. Massie, J. K. Salisbury, *et al.*, "The Phantom haptic interface: A device for probing virtual objects," in *Proceedings of the ASME winter annual meeting, symposium on haptic interfaces for virtual environment and teleoperator systems*, vol. 55, pp. 295–300, 1994.

[88] S. Kim, S. Hasegawa, Y. Koike, and M. Sato, "Tension based 7-DOF force feedback device: SPIDAR-G," in *Proceedings of IEEE Virtual Reality*, pp. 283–284, 2002.

[89] M. Bouzit, G. Burdea, G. Popescu, and R. Boian, "The Rutgers Master II-new design force-feedback glove," *IEEE/ASME Transactions on Mechatronics*, vol. 7, no. 2, pp. 256–263, 2002.

[90] J. H. Killebrew, S. J. Bensmaia, J. F. Dammann, P. Denchev, S. S. Hsiao, J. C. Craig, and K. O. Johnson, "A dense array stimulator to generate arbitrary spatio-temporal tactile stimuli," *Journal of neuroscience methods*, vol. 161, no. 1, pp. 62–74, 2007.

[91] C. H. King, M. O. Culjat, M. L. Franco, J. W. Bisley, E. Dutson, and W. S. Grundfest, "Optimization of a pneumatic balloon tactile display for robot-assisted surgery based on human perception," *IEEE Transactions on Biomedical Engineering*, vol. 55, no. 11, pp. 2593–2600, 2008.

[92] M. Miyakami, K. A. Murata, and H. Kajimoto, "Hapballoon: Wearable haptic balloon-based feedback device," in *Proceedings of ACM Special Interest Group on Computer Graphics (SIGGRAPH) Asia Emerging Technologies*, pp. 17–18, 2019.

[93] M. Culjat, C. H. King, M. Franco, J. Bisley, W. Grundfest, and E. Dutson, "Pneumatic balloon actuators for tactile feedback in robotic surgery," *Industrial Robot*, vol. 35, no. 5, pp. 449–455, 2008.

[94] A. A. Stanley, J. C. Gwilliam, and A. M. Okamura, "Haptic jamming: A deformable geometry, variable stiffness tactile display using pneumatics and particle jamming," in *Proceedings of IEEE World Haptics Conference (WHC)*, pp. 25–30, 2013.

[95] K. Minamizawa, S. Fukamachi, H. Kajimoto, N. Kawakami, and S. Tachi, "Gravity grabber: wearable haptic display to present virtual mass sensation," in *Proceedings of ACM Special Interest Group on Computer Graphics (SIGGRAPH) Emerging Technologies*, pp. 8–11, 2007.

[96] M. Kitagawa, D. Dokko, A. M. Okamura, and D. D. Yuh, "Effect of sensory substitution on suture-manipulation forces for robotic surgical systems," *Journal of Thoracic and Cardiovascular Surgery*, vol. 129, no. 1, pp. 151–158, 2005.

[97] N. Cutler, M. Balicki, M. Finkelstein, J. Wang, P. Gehlbach, J. McGready, I. Iordachita, R. Taylor, and J. T. Handa, "Auditory force feedback substitution improves surgical precision during simulated ophthalmic surgery," *Investigative ophthalmology & visual science*, vol. 54, no. 2, pp. 1316–1324, 2013.

[98] A. A. Yusof, T. Kawamura, and H. Yamada, "Evaluation of construction robot telegrasping force perception using visual, auditory and force feedback integration.," *Journal of Robotics and Mechatronics*, vol. 24, no. 6, pp. 949–957, 2012.

[99] M. Tavakoli, A. Aziminejad, R. Patel, and M. Moallem, "Methods and mechanisms for contact feedback in a robot-assisted minimally invasive environment," *Surgical Endoscopy and Other Interventional Techniques*, vol. 20, no. 10, pp. 1570–1579, 2006.

[100] T. Akinbiyi, C. E. Reiley, S. Saha, D. Burschka, C. J. Hasser, D. D. Yuh, and A. M. Okamura, "Dynamic augmented reality for sensory substitution in robot-assisted surgical systems," in *Proceedings of the International Conference of the IEEE Engineering in Medicine and Biology Society*, pp. 567–570, 2006.

[101] C. E. Reiley, T. Akinbiyi, D. Burschka, D. C. Chang, A. M. Okamura, and D. D. Yuh, "Effects of visual force feedback on robot-assisted surgical task performance," *Journal of Thoracic and Cardiovascular Surgery*, vol. 135, no. 1, pp. 196–202, 2008.

[102] J. Dargahi, S. Najarian, and R. Ramezanifard, "Graphical display of tactile sensing data with application in minimally invasive surgery," *Canadian Journal of Electrical and Computer Engineering*, vol. 32, no. 3, pp. 151–155, 2007.

[103] A. Talasaz, A. L. Trejos, and R. V. Patel, "The role of direct and visual force feedback in suturing using a 7-DOF dual-arm teleoperated system," *IEEE Transactions on Haptics*, vol. 10, no. 2, pp. 276–287, 2016.

[104] T. Debus, T. Becker, P. Dupont, T. J. Jang, and R. D. Howe, "Multichannel vibrotactile display for sensory substitution during teleoperation," in *Telemanipulator and Telepresence Technologies VIII*, vol. 4570, pp. 42–49, International Society for Optics and Photonics, 2002.

[105] M. J. Massimino and T. B. Sheridan, "Sensory substitution for force feedback in teleoperation," *IFAC Proceedings Volumes*, vol. 25, no. 9, pp. 109–114, 1992.

[106] J. Black, *Biological performance of materials: fundamentals of biocompatibility*. CRC Press, 2005.

[107] D. H. Kim, N. Lu, R. Ghaffari, Y. S. Kim, S. P. Lee, L. Xu, J. Wu, R. H. Kim, J. Song, Z. Liu, *et al.*, "Materials for multifunctional balloon catheters with capabilities in cardiac electrophysiological mapping and ablation therapy," *Nature materials*, vol. 10, no. 4, pp. 316–323, 2011.

[108] G. B. Limentani, M. C. Ringo, F. Ye, M. L. Bergquist, and E. O. McSorley, "Beyond the t-test: statistical equivalence testing," *Analytical chemistry*, vol. 77, no. 11, pp. 221–226, 2005.

[109] V. V. Lulevich, D. Andrienko, and O. I. Vinogradova, "Elasticity of polyelectrolyte multilayer microcapsules," *The Journal of chemical physics*, vol. 120, no. 8, pp. 3822–3826, 2004.

[110] M. Shanahan, "A novel test for the appraisal of solid/solid interfacial interactions," *The Journal of Adhesion*, vol. 63, no. 1-3, pp. 15–29, 1997.

[111] M. E. Shanahan, "Adhesion of a liquid-filled spherical membrane," *The Journal of Adhesion*, vol. 79, no. 10, pp. 881–891, 2003.

[112] J. Lemaitre and J. L. Chaboche, *Mechanics of solid materials*. Cambridge University press, 1994.

[113] V. Lulevich, T. Zink, H. Y. Chen, F. T. Liu, and G. Y. Liu, "Cell mechanics using atomic force microscopy-based single-cell compression," *Langmuir*, vol. 22, no. 19, pp. 8151–8155, 2006.

[114] M. A. Greminger and B. J. Nelson, "Vision-based force measurement," *IEEE Transactions on Pattern Analysis and Machine Intelligence*, vol. 26, no. 3, pp. 290–298, 2004.

[115] L. Meli, C. Pacchierotti, G. Salvietti, F. Chinello, M. Maisto, A. De Luca, and D. Prattichizzo, "Combining wearable finger haptics and augmented reality: User evaluation using an external camera and the microsoft hololens," *IEEE Robotics and Automation Letters*, vol. 3, no. 4, pp. 4297–4304, 2018.

[116] C. Gaudeni, L. Meli, L. A. Jones, and D. Prattichizzo, "Presenting surface features using a haptic ring: A psychophysical study on relocating vibrotactile feedback," *IEEE Transactions on Haptics*, vol. 12, no. 4, pp. 428–437, 2019.

[117] O. Ariza, P. Lubos, F. Steinicke, and G. Bruder, "Ring-shaped haptic device with vibrotactile feedback patterns to support natural spatial interaction," in *Proceedings of the 25th International Conference on Artificial Reality and Telexistence and 20th Eurographics Symposium on Virtual Environments*, pp. 175–181, 2015.

[118] Precision Microdrives, "Model No. 304-002 4mm Vibration Motor - 8mm Type Datasheet."

[119] K. H. Park, B. H. Kim, and S. Hirai, "Development of a soft-fingertip and its modeling based on force distribution," in *Proceedings of IEEE International Conference on Robotics and Automation*, vol. 3, pp. 3169–3174, 2003.

[120] T. Lisini Baldi, S. Scheggi, L. Meli, M. Mohammadi, and D. Prattichizzo, "GESTO: A glove for enhanced sensing and touching based on inertial and magnetic sensors for hand tracking and cutaneous feedback," *IEEE Transactions on Human-Machine Systems*, vol. 47, no. 6, pp. 1066–1076, 2017.

[121] C. Lee, M. Kim, Y. J. Kim, N. Hong, S. Ryu, H. J. Kim, and S. Kim, "Soft robot review," *International Journal of Control, Automation and Systems*, vol. 15, no. 1, pp. 3–15, 2017.

[122] S. Kim, C. Laschi, and B. Trimmer, "Soft robotics: a bioinspired evolution in robotics," *Trends in biotechnology*, vol. 31, no. 5, pp. 287–294, 2013.

[123] J. Hughes, U. Culha, F. Giardina, F. Guenther, A. Rosendo, and F. Iida, "Soft manipulators and grippers: A review," *Frontiers in Robotics and AI*, vol. 3, p. 69, 2016.

[124] Y. Hwang, O. H. Paydar, and R. N. Candler, "Pneumatic microfinger with balloon fins for linear motion using 3D printed molds," *Sensors and Actuators A: Physical*, vol. 234, pp. 65–71, 2015.

[125] C. Eppner, R. Deimel, J. Alvarez-Ruiz, M. Maertens, and O. Brock, "Exploitation of environmental constraints in human and robotic grasping," *The International Journal of Robotics Research*, vol. 34, no. 7, pp. 1021–1038, 2015.

[126] M. Pozzi, G. Salvietti, J. Bimbo, M. Malvezzi, and D. Prattichizzo, "The closure signature: A functional approach to model underactuated compliant robotic hands," *IEEE Robotics and Automation Letters*, vol. 3, no. 3, pp. 2206–2213, 2018.

[127] J. Bimbo, E. Turco, M. Ghazaei Ardakani, M. Pozzi, G. Salvietti, V. Bo, M. Malvezzi, and D. Prattichizzo, "Exploiting robot hand compliance and environmental constraints for edge grasps," *Frontiers in Robotics and AI*, vol. 6, p. 135, 2019.

[128] R. Deimel and O. Brock, "A novel type of compliant and underactuated robotic hand for dexterous grasping," *The International Journal of Robotics Research*, vol. 35, no. 1-3, pp. 161–185, 2016.

[129] F. Vigni, E. Knoop, D. Prattichizzo, and M. Malvezzi, "The role of closed-loop hand control in handshaking interactions," *IEEE Robotics and Automation Letters*, vol. 4, no. 2, pp. 878–885, 2019.

[130] C. Piazza, M. G. Catalano, S. B. Godfrey, M. Rossi, G. Grioli, M. Bianchi, K. Zhao, and A. Bicchi, "The SoftHand Pro-H: A hybrid body-controlled, electrically powered hand prosthesis for daily living and working," vol. 24, no. 4, pp. 87–101, 2017.

[131] W. Wan, K. Harada, and F. Kanehiro, "Planning grasps for assembly tasks," *arXiv preprint arXiv:1903.01631*, 2019.

[132] P. J. Sanz, A. Requena, J. M. Inesta, and A. P. Del Pobil, "Grasping the not-so-obvious: vision-based object handling for industrial applications," *IEEE Robotics & Automation Magazine*, vol. 12, no. 3, pp. 44–52, 2005.

[133] C. Della Santina, V. Arapi, G. Averta, F. Damiani, G. Fiore, A. Settimi, M. G. Catalano, D. Bacciu, A. Bicchi, and M. Bianchi, "Learning from humans how to grasp: a data-driven architecture for autonomous grasping with anthropomorphic soft hands," *IEEE Robotics and Automation Letters*, vol. 4, no. 2, pp. 1533–1540, 2019.

[134] H. Dang, J. Weisz, and P. K. Allen, "Blind grasping: Stable robotic grasping using tactile feedback and hand kinematics.," in *Proceedings of IEEE International Conference on Robotics and Automation*, pp. 5917–5922, 2011.

[135] T. Kim, D. M. Kim, B. J. Lee, and J. Lee, "Soft and deformable sensors based on liquid metals," *IEEE Sensors Journal*, vol. 19, no. 19, p. 4250, 2019.

[136] S. Suprapto, A. Setiawan, H. Zakaria, W. Adiprawita, and B. Supartono, "Low-cost pressure sensor matrix using velostat," in *Proceedings of International Conference on Instrumentation, Communications, Information Technology, and Biomedical Engineering (ICICI-BME)*, pp. 137–140, 2017.

[137] L. Wang and Z. Wang, "Mechanoreception for soft robots via intuitive body cues," *Soft robotics*, vol. 7, no. 2, pp. 198–217, 2020.

[138] A. Misaki, K. Imanishi, S. Takasugi, M. Wada, S. Fukagawa, and M. Furue, "Body pressure sensing mattress for bedsore prevention," *SEI technical review*, vol. 78, pp. 95–99, 2014.

[139] C. H. Kuo, H. C. Chou, and S. Y. Tasi, "Pneumatic sensor: A complete coverage improvement approach for robotic cleaners," *IEEE Transactions on Instrumentation and Measurement*, vol. 60, no. 4, pp. 1237–1256, 2011.

[140] H. Nozawa, S. Lee, J. Kim, and K. Inoue, "Human-robot cooperation for heavy object manipulation based on sensing pneumatic pressure in air cushions," in *Proceedings of IEEE/ASME International Conference on Advanced Intelligent Mechatronics (AIM)*, pp. 391–396, 2012.

[141] Y. Akamatsu, T. Nakamura, and Y. Kusaka, "Development of a soft manipulator with flexible joints using smart fluid and pneumatics cushion for collision with human," in *Proceedings of IEEE/ASME International Conference on Advanced Intelligent Mechatronics*, pp. 1–6, 2007.

[142] D. Gong, R. He, J. Yu, and G. Zuo, "A pneumatic tactile sensor for co-operative robots," *IEEE Sensors Journal*, vol. 17, no. 11, p. 2592, 2017.

[143] M. Russo, M. Ceccarelli, B. Corves, M. Hüsing, M. Lorenz, D. Cafolla, and G. Carbone, "Design and test of a gripper prototype for horticulture products," *Robotics and Computer-Integrated Manufacturing*, vol. 44, pp. 266–275, 2017.

[144] Soft Robotics Toolkit, "Soft gripper fabrication guide," 2016.

[145] D. Pamplona and D. Mota, "Numerical and experimental analysis of inflating a circular hyperelastic membrane over a rigid and elastic foundation," *International Journal of Mechanical Sciences*, vol. 65, no. 1, pp. 18–23, 2012.

[146] M. Quigley, K. Conley, B. P. Gerkey, J. Faust, T. Foote, J. Leibs, R. Wheeler, and A. Y. Ng, "Ros: an open-source robot operating system," in *ICRA Workshop on Open Source Software*, 2009.

[147] B. Calli, A. Walsman, A. Singh, S. Srinivasa, P. Abbeel, and A. M. Dollar, "Benchmarking in manipulation research: Using the Yale-CMU-Berkeley object and model set," *IEEE Robotics Automation Magazine*, vol. 22, no. 3, pp. 36–52, 2015.

[148] L. Biagiotti, C. Melchiorri, P. Tiezzi, and G. Vassura, "Modelling and identification of soft pads for robotic hands," in *Proceedings of IEEE/RSJ International Conference on Intelligent Robots and Systems*, pp. 2786–2791, 2005.

[149] D. Kragic and K. Daniilidis, "3-D vision for navigation and grasping," in *Springer Handbook of Robotics*, pp. 811–824, 2016.

[150] R. M. Murray, *A mathematical introduction to robotic manipulation*. CRC press, 2017.

[151] H. I. Christensen and G. D. Hager, "Sensing and estimation," in *Springer Handbook of Robotics*, pp. 91–112, 2016.

[152] I. Hussain, F. Renda, M. I. Zubair, M. Malvezzi, G. Salvietti, L. Seneviratne, D. Gan, and D. Prattichizzo, "Modeling and prototyping of an underactuated gripper exploiting joint compliance and modularity," *IEEE Robotics and Automation Letters*, vol. 3, no. 4, pp. 2854–2861, 2018.

[153] M. Pozzi, E. Miguel, R. Deimel, M. Malvezzi, B. Bickel, O. Brock, and D. Prattichizzo, "Efficient FEM-based simulation of soft robots modeled as kinematic chains," in *Proceedings of IEEE International Conference on Robotics and Automation*, pp. 1–8, 2018.

[154] J. C. Case, E. L. White, and R. K. Kramer, "Soft material characterization for robotic applications," *Soft Robotics*, vol. 2, no. 2, pp. 80–87, 2015.

[155] N. Elango and A. Faudzi, "A review article: investigations on soft materials for soft robot manipulations," *The International Journal of Advanced Manufacturing Technology*, vol. 80, no. 5-8, pp. 1027–1037, 2015.

[156] P. Martins, R. Natal Jorge, and A. Ferreira, "A comparative study of several material models for prediction of hyperelastic properties: Application to silicone-rubber and soft tissues," *Strain*, vol. 42, no. 3, pp. 135–147, 2006.

[157] S. N. A. M. Noor and J. Mahmud, "Modelling and computation of silicone rubber deformation adapting neo-hookean constitutive equation," in *Proceedings of IEEE Fifth International Conference on Communication Systems and Network Technologies*, pp. 1323–1326, 2015.

[158] M. Mooney, "A theory of large elastic deformation," *Journal of Applied Physics*, vol. 11, no. 9, pp. 582–592, 1940.

[159] R. W. Ogden, "Large deformation isotropic elasticity–on the correlation of theory and experiment for incompressible rubberlike solids," *Proceedings of the Royal Society of London. A. Mathematical and Physical Sciences*, vol. 326, no. 1567, pp. 565–584, 1972.

[160] J. Hill, "Exact integrals and solutions for finite deformations of the incompressible varga elastic materials," *London Mathematical Society Lecture Note Series*, pp. 160–200, 2001.

[161] O. H. Yeoh, "Some forms of the strain energy function for rubber," *Rubber Chemistry and technology*, vol. 66, no. 5, pp. 754–771, 1993.

[162] A. Gent, "A new constitutive relation for rubber," *Rubber chemistry and technology*, vol. 69, no. 1, pp. 59–61, 1996.

[163] R. Lewandowski and B. Chorążyczewski, "Identification of the parameters of the Kelvin–Voigt and the Maxwell fractional models, used to modeling of viscoelastic dampers," *Computers & structures*, vol. 88, no. 1-2, pp. 1–17, 2010.

[164] D. Steck, J. Qu, S. Kordmahale, D. Tscharnuter, A. Muliana, and J. Kameoka, "Mechanical responses of Ecoflex silicone rubber: Compressible and incompressible behaviors," *Journal of Applied Polymer Science*, vol. 136, no. 5:47025, 2019.

[165] "COMSOL Multiphysics, Structural Mechanics Module User's Guide," 2017.

[166] A. Pal, D. Goswami, and R. V. Martinez, "Elastic energy storage enables rapid and programmable actuation in soft machines," *Advanced Functional Materials*, vol. 30, no. 1:1906603, 2019.

[167] H. K. Yap, J. C. H. Goh, and R. C. H. Yeow, "Design and characterization of soft actuator for hand rehabilitation application," in *Proceedings of the 6th European Conference of the International Federation for Medical and Biological Engineering*, pp. 367–370, 2015.

[168] C. Gaudeni, L. Meli, and D. Prattichizzo, "A novel pneumatic force sensor for robot-assisted surgery," in *Proceedings of International Conference on Human Haptic Sensing and Touch Enabled Computer Applications (EuroHaptics)*, pp. 587–599, 2018.

[169] C. Gaudeni and D. Prattichizzo, "A mathematical model of the pneumatic force sensor for robot-assisted surgery," in *Proceedings of IEEE World Haptics Conference (WHC)*, pp. 598–603, 2019.

[170] C. Gaudeni, T. L. Baldi, G. M. Achilli, M. Mandalà, and D. Prattichizzo, "Instrumenting hand-held surgical drills with a pneumatic sensing cover for haptic feedback," in *Proceedings of International Conference on Human Haptic Sensing and Touch Enabled Computer Applications (EuroHaptics)*, pp. 398–406, 2020.

[171] C. Gaudeni, M. Pozzi, Z. Iqbal, M. Malvezzi, and D. Prattichizzo, "Grasping with the Softpad, a soft sensorized surface for exploiting environmental constraints with rigid grippers," *IEEE Robotics and Automation Letters*, vol. 5, no. 3, pp. 3884–3891, 2020.

[172] M. Pozzi, C. Gaudeni, Z. Iqbal, D. Prattichizzo, and M. Malvezzi, "Modeling a sensorized soft layer for adding compliance to the environment in robotic manipulation," in *Proceedings of The International Conference of IFToMM ITALY*, pp. 370–377, 2020.